NPL
National Physical Laboratory

The Use of Finite Element Methods for Design with Adhesives
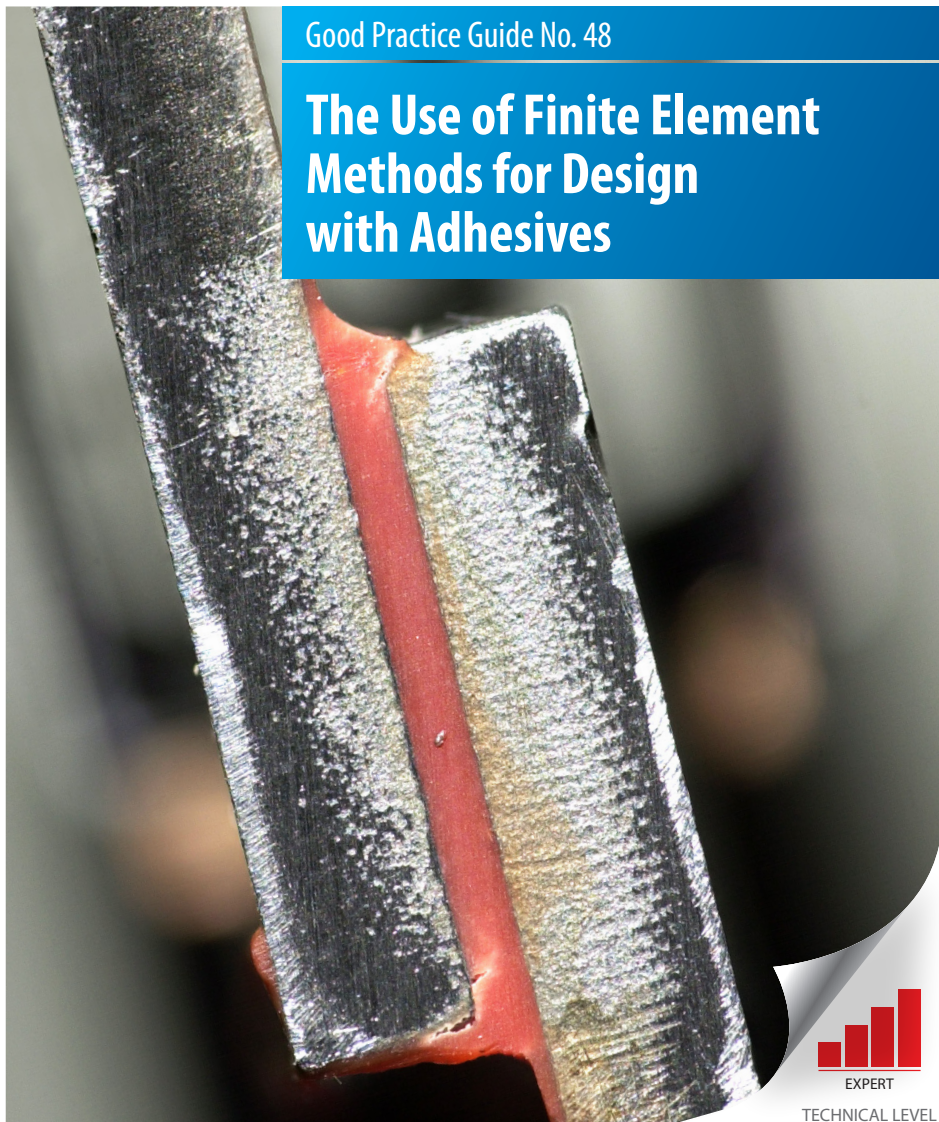
EXPERT

TECHNICAL LEVEL

Department for
Business, Energy
& Industrial Strategy

FUNDED BY BEIS

The National Physical Laboratory (NPL)

NPL is the UK's National Measurement Institute, and is a world-leading centre of excellence in developing and applying the most accurate measurement standards, science and technology available.

NPL's mission is to provide the measurement capability that underpins the UK's prosperity and quality of life.

NPL Authors and Contributors

Greg Dean
Louise Crocker

Find out more about NPL measurement training at **www.npl.co.uk/training** or our e-learning Training Programme at **www.npl.co.uk/e-learning**

National Physical Laboratory
Hampton Road
Teddington
Middlesex
TW11 0LW
United Kingdom

Telephone: +44 (0)20 8977 3222
e-mail: training@npl.co.uk
www.npl.co.uk

Abstract/Foreword

A finite element analysis is able to determine stress and strain distributions throughout a bonded structure resulting from an applied force or displacement. It is possible to calculate the stiffness of the joint and to locate regions of stress and strain concentration where failure is expected to initiate. Using a suitably fine mesh the influence of geometrical features, such as the size and shape of fillets at the ends of the adhesive layer, on stress and strain distributions can be evaluated. The relevance of finite element methods to the design of adhesive joints is therefore apparent. The accuracy of design calculations is however dependent upon the validity of the materials models used in the analysis to describe the deformation behaviour of the adhesive and adherends and the availability of suitable materials property data for these models.

This Good Practice Guide describes a range of materials models that are suitable for use with rigid (glassy) adhesives and adherends. Reference is made to models for linear elastic and viscoelastic behaviour, but emphasis is given to elastic-plastic models that are needed to describe the non-linear behaviour of tough adhesives. Some of the limitations in the use of these models with rubber-toughened adhesives are explained and illustrated with extensive data on a toughened epoxy.

Selected test methods for bulk and joint specimens are described that can be used to determine the property data and parameters required by these models. Emphasis is given to the determination of properties over a wide range of strain rate to enable predictions to be made of performance under impact loading. Procedures for analysing experimental results to obtain the model parameters are explained.

Guidance on setting up a finite element analysis is also given regarding meshing the geometry of a joint and selection of a suitable method of solution. The application of finite element analyses to some common joint geometries is illustrated in the Appendix. Comparisons are made here of force/extension curves and stress and strain distributions calculated using different models and solvers. The influences of simplifying assumptions regarding flow behaviour and strain-rate are also illustrated.

Acknowledgements

Contents

Chapter 1

Introduction

- Introduction
- Nomenclature

Introduction

Finite element analysis is a computational tool that can be used for calculating forces, deformations, stresses and strains throughout a bonded structure. The geometry of the structure is represented by a series of nodes that define the corners of a 2 or 3 dimensional array of elements. A loading situation is simulated by applying constraints and forces or displacements at the boundary of the structure. The resulting forces, displacements, stresses and strains throughout the structure are then calculated by solving the equations (constitutive laws) that describe the deformation behaviour of the materials comprising the structure whilst maintaining continuity of displacement at all the nodes. These are solved for each incremental increase in the applied force or displacement. As a result of the analysis, the following quantities can be calculated:

- the deflection of any point (node) in the structure as a function of the applied force (a force/displacement curve)
- components of stress or strain in any element at particular levels of applied force or displacement. These are often displayed as contour maps.

The power of finite element analysis is now apparent since these predictions can be made at any point in the structure including within the adhesive layer. Furthermore, the complex geometry of the bond line can be accurately described by the element mesh so the influence of geometrical features, such as the shape of fillets and boundaries with adherends, on joint performance is accounted for in the analysis. This is particularly important in the design of adhesive joints because these features are usually associated with regions of stress and strain concentration at which joint failure will generally initiate.

From the above, it is clearly possible to determine the stiffness of the joint. This prediction involves the generation of small strains in the materials and an elastic analysis is satisfactory with suitable elastic properties for the adhesive and adherends. The prediction of joint failure is more complicated. Untoughened, thermosetting adhesives are generally brittle materials that will fail at relatively small strains by the initiation and propagation of a crack. The behaviour of these materials is essentially elastic to failure which can, in principle, be predicted if the failure criterion is known.

Most commercial adhesives are, however, rubber toughened. The rubber phase occurs as finely dispersed particles, which enhance plastic deformation in the matrix polymer between particles. Under stress states where there is a significant component of hydrostatic stress, this process is further enhanced by the cavitation of the rubber particles. These materials therefore sustain relatively large strains (>5%) with extensive plastic deformation prior to failure. Prediction of joint performance under these circumstances requires the use of models that describe the non-linear mechanical behaviour of the adhesive (and possibly the

adherends also). For glassy adhesives (operating at temperatures below the glass transition temperature), elastic-plastic models are employed in finite element systems for this purpose.

There are several models available based on different criteria for plastic deformation. Predictions of joint performance at large strains close to joint failure depend on the model used, and the accuracy of these predictions is uncertain. There is therefore interest in developing new models with higher predictive accuracy. This is motivated by the need to predict the performance of bonded structures under impact loading so that the load and absorbed energy prior to failure can be calculated. This requires proper consideration of the dependence of plastic deformation of the adhesive on the applied strain rate and the determination of relevant rate-dependent properties. For the prediction of failure, stress and strain distributions in the adhesive need to be accurately calculated and a failure criterion for the adhesive needs to be established. These topics are still subjects of ongoing research. However, using available models, finite element analyses are able to predict the location of regions of stress or strain concentration where failure will probably initiate. These calculations then allow the influence of factors, such as the geometry of the ends of the adhesive layer, on stress and strain levels to be investigated. Whilst these calculations may have uncertain quantitative accuracy, they can be used to optimise joint performance through choice of joint dimensions and geometry.

In Chapter 2 of this Guide, the various materials models that are commonly used to describe the deformation behaviour of adhesives are explained, and the materials properties and parameters required for the application of these models are introduced. In Chapter 3, measurement methods are described that can be used to determine these properties and parameters. These procedures are illustrated using selected results from extensive measurements made on a rubber-toughened adhesive. Chapter 4 demonstrates how the property data and parameters required by a finite element analysis are determined from experimental results. Chapter 5 describes how a finite element analysis is set up, and results of analyses of some common joint geometries are discussed in the Appendix. A discussion of possible criteria for the initiation of failure in an adhesive joint is given in Chapter 6.

Nomenclature

Definitions of all symbols appearing in this guide are provided below.

σ_{ij}, ε_{ij}	components of the stress and strain tensor respectively
σ_i, ε_i	components of principal stress and strain respectively
σ', ε'	engineering values of stress and strain respectively
ε'_t	engineering value of transverse strain
σ'_T, ε'_T	engineering values of stress and strain respectively under tension
σ, ε	true values of stress and strain respectively
σ_T, σ_S, σ_C	true stresses under tension, shear and compression respectively
ε_T, ε_S, ε_C	true values of strain under tension, shear and compression respectively
ε^e, ε^p	true values of the elastic and plastic components of strain respectively
ε_T^e	true value of the elastic strain under tension
ε_t	true value of transverse strain
ε_i^p	principal plastic strains (i=1, 2 or 3)
ε_t^e, ε_t^p	true elastic and plastic components of transverse strain under uniaxial tension
ε_T^p, ε_S^p, ε_C^p	true plastic strains under tension, shear and compression respectively
γ, γ^p	shear strain and plastic component of the shear strain measured in a shear test
σ_e, t, q	terms for the effective shear component of stress
σ_m, -p	terms for the hydrostatic component of stress
σ_o, ε_o^p	effective shear yield stress and plastic strain respectively
ε_e^p	the effective plastic strain
E, G, K	the Young's, shear and bulk modulus respectively
ν'	Poisson's ratio calculated from engineering strains
ν	Poisson's ratio calculated from true strains
ν^e	the elastic component of Poisson's ratio

ν^p, ν_C^p the plastic components of Poisson's ratio under tension and compression respectively

μ, β hydrostatic stress sensitivity parameters in the linear Drucker-Prager yield criterion

λ, a hydrostatic stress sensitivity parameters in the exponent Drucker-Prager yield criterion

p_t hardening parameter in the exponent Drucker-Prager yield criterion

G, F the flow potential for linear and exponent forms of the Drucker-Prager model respectively

μ', λ', Ψ parameters in the flow potential for non-associated flow

$\dot{\varepsilon}$, $\dot{\varepsilon}_T^p$ strain rate and tensile plastic strain rate respectively

σ_f, σ_y, ε_r, n, α parameters in a function used to model plastic strain hardening

σ_{fo}, σ_{yo}, b, c parameters in an equation used to model rate-dependent plasticity

Chapter 2

Materials Models

- Deformation of tough adhesives
- Elastic behaviour
- Models for non-linear behaviour
- Rate-dependent plasticity

Deformation of tough adhesives

Figure 1 shows a stress/strain curve for a toughened epoxy adhesive measured under uniaxial tension. The stresses and strains are true values (see equations (5) and (6)). The plot shows:

- a region of linear elastic behaviour at small strains
- the onset of non-linear behaviour at a stress σ_y. In elastic-plastic models, this stress marks the beginning of plastic deformation and σ_y is the initial yield stress
- a region of non-linear deformation leading to a plateau in the stress. In elastic-plastic models, this region is attributed to strain hardening
- a region prior to failure where the stress changes very little with increasing strain. This is termed the flow region.

The data shown in Figure 1 are a significant proportion of what are required for a stress analysis. The precise data requirements depend on assumptions of materials behaviour. Materials models and data requirements for a variety of types of behaviour are considered next.
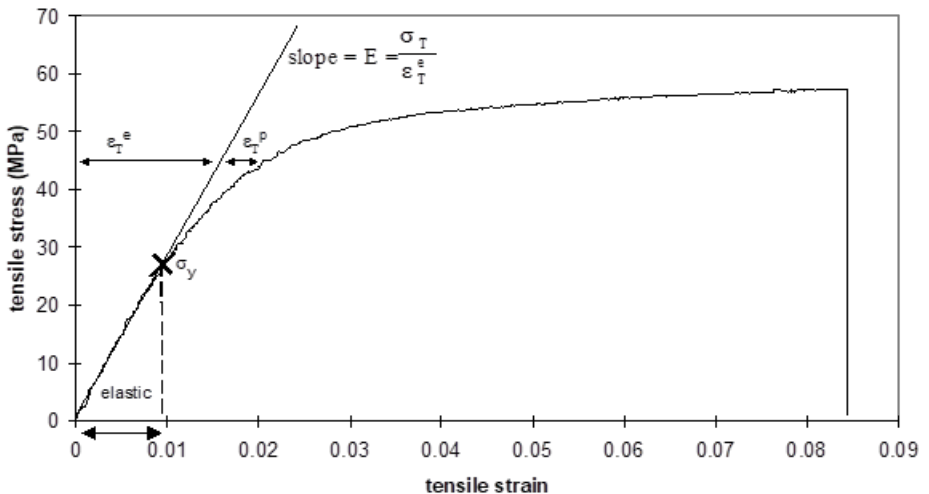

Figure 1. *Tensile stress/strain curve for the toughened epoxy adhesive.*

Elastic behaviour

Stress and strain levels up to the initial yield stress σ_y in Figure 1 define the region of linear, elastic behaviour.

Strictly, since adhesives (as with all polymers) are viscoelastic materials, the behaviour here is linear viscoelastic. The implications of this will be considered later in this section.

Where behaviour can be assumed to be linear elastic, stress and strain components, σ_{ij} and ε_{kl} respectively, are related by the tensor equation

$$\sigma_{ij} = C_{ijkl}\varepsilon_{kl} \tag{1}$$

where C_{ijkl} are components of the stiffness tensor. For isotropic materials, these stiffness components are related to only two elastic properties of the material. These properties are usually chosen to be the Young's modulus E and Poisson's ratio ν^e, and they can be conveniently measured using tensile tests on bulk specimens as described in Chapter 3. Alternatively, the Young's modulus and shear modulus G can be measured.

Extension to linear viscoelasticity

Polymers, and hence adhesives, are viscoelastic materials. Properties will therefore depend upon the timescale over which measurements are made. For glassy adhesives at temperatures that are well below their glass-to-rubber transition temperature, these changes will be small in the timescale of most experiments. As the temperature approaches the glass transition temperature, the effects arising from viscoelasticity will be more evident. In tests under constant deformation rate (crosshead speed), the initial slope of the stress/strain curve (the modulus) will depend upon the strain rate. Associated with this, there will be some slight curvature even at small strains where behaviour is usually assumed to be linear. Viscoelastic effects are also evident in other tests. Under constant stress (creep) or constant strain (stress relaxation) moduli will decrease with time. In dynamic mechanical tests, moduli will increase with frequency, and damping properties will be apparent through a phase difference between the stress and strain cycles.

It is possible to take account of viscoelasticity in an analysis. The most rigorous approach is to use a creep or stress relaxation function to characterise time-dependent behaviour and calculate the response to a time-varying applied load or displacement by assuming superposition of strain or stress increments respectively. Recovery, arising from the removal of load or the reversal of displacement, is taken care of by adding the response from negative

stresses or strains respectively. An approximation for monotonic loading is possible by expressing Young's modulus as a function of strain rate, obtained from constant strain rate tests, and using an elastic analysis with the appropriate modulus for each element depending on the strain rate seen by that element. A "rate-dependent elasticity model" such as this is not commonly available in finite element systems so it would be necessary to code a user-defined materials model (UMAT) for use with an FE solver.

Materials models for dynamic mechanical behaviour are available and enable stiffness and damping calculations to be made in a bonded structure in response to vibrations or the excitation of resonances. Data for the dynamic modulus and loss factor in tension are needed either at a single frequency or, for higher accuracy, over a range of frequencies. A value for Poisson's ratio, assumed to be real, can be taken from a tensile test under constant strain rate without any significant loss of accuracy.

Models for non-linear behaviour

A brief introduction to elastic-plastic models

At stress and strain levels above the limit for linear behaviour, relationships between stress and strain are non-linear. The non-linear behaviour of plastics materials is generally interpreted as enhanced viscoelastic deformation arising from an increase in molecular mobility caused by the application of stresses above the limit for linear behaviour. At these stress levels, relaxation times are reduced leading to enhanced creep and stress relaxation. Satisfactory models of this non-linear viscoelasticity have yet to be developed, and FE packages generally consider material non-linearity in rigid materials in terms of elastic-plastic models that were developed for metals.

With elastic-plastic models, calculations of stress and strain distributions at low strains are based on linear elasticity. The onset of non-linearity is then ascribed to plastic deformation and occurs at a stress level regarded as the first yield stress. The subsequent increase in stress with strain is associated with the effects of strain hardening. In this non-linear region, the total strain ε_{ij} is considered to be the sum of a recoverable elastic component ε_{ij}^e and a plastic component ε_{ij}^p, which is non-recoverable. Thus

$$\varepsilon_{ij} = \varepsilon_{ij}^e + \varepsilon_{ij}^p \qquad (2)$$

Stress analysis calculations then involve the use of multiaxial yield criteria and a flow law. Some of the yield criteria that have been used to model plastic deformation in adhesives are described in the following sections.

The yield criterion relates components of applied stress field to material parameters after the onset of yielding. The material parameters will depend upon the plastic strain for a strain hardening material. This is a material having a range of yield stress varying from an initial value σ_y, marking the onset of non-linearity, to a maximum value corresponding to the flow region (see Figure 1).

The calculation of plastic strain components is achieved in plasticity theory using a flow rule (see equation (19)), which relates increments of plastic strain to a plastic flow potential. If the flow behaviour for a particular material is such that the flow potential can be identified with the yield function then this is termed associated flow. In general, this will be an approximation and the extra information needed to characterise non-associated flow is described later.

In order to calculate some of the parameters in elastic-plastic models, it is necessary to select stress values from different tests under the same state of yielding. This requires the definition of an effective plastic strain (equation (26)), and equivalent stresses are then a set of stresses that characterise stress states having the same effective plastic strain.

The von Mises criterion

The most simple yield criterion interprets yielding as a purely shear deformation process which occurs when the effective shear stress σ_e reaches a critical value. This effective stress is defined in terms of principal stress components σ_i (i = 1, 2 or 3) by

$$\sigma_e = \left\{ \frac{1}{2} [(\sigma_1 - \sigma_2)^2 + (\sigma_2 - \sigma_3)^2 + (\sigma_3 - \sigma_1)^2] \right\}^{1/2} \tag{3}$$

The von Mises criterion then relates σ_e to the yield stress in tension σ_T by

$$\sigma_e = \sigma_T \tag{4}$$

The tensile yield stress σ_T is now a material parameter and has a minimum value, which denotes the limit of elastic behaviour and the start of plastic deformation (see Figure 1) and will increase tensile plastic strain ε_T^p. The function $\sigma_T(\varepsilon_T^p)$ is called the tensile strain hardening function.

In equations (2), (3) and (4) and the equations that follow, stresses σ and strains ε are true values and are related to nominal (engineering) values σ'_T and ε'_T based on the original specimen dimensions by

$$\sigma_T = \frac{\sigma'_T}{(1 - v'\varepsilon'_T)^2} \tag{5}$$

and

$$\varepsilon_T = \ln(1 + \varepsilon'_T) \tag{6}$$

It is evident from equations (5) and (6) that true and engineering values of stress and strain are effectively the same at strains below about 0.05. The need to calculate true values therefore only arises in analyses involving relatively large strain plasticity.

It follows from equation (2) that

$$\varepsilon_T = \varepsilon^e_T + \varepsilon^p_T = \frac{\sigma_T}{E} + \varepsilon^p_T \tag{7}$$

$$\varepsilon_t = \varepsilon^e_t + \varepsilon^p_t = \frac{-v^e\sigma_T}{E} + \varepsilon^p_t \tag{8}$$

$$v' = -\frac{\varepsilon'_t}{\varepsilon'_T} \tag{9}$$

and

$$v = -\frac{\varepsilon_t}{\varepsilon_T} \tag{10}$$

where ε'_t and ε_t are negative quantities.

The von Mises criterion predicts that the tensile yield stress, shear yield stress and compressive yield stress are related by

$$\sigma_T = \sigma_C = \sqrt{3}\sigma_S \tag{11}$$

Tests on adhesives under additional stress states such as shear and compression reveal that yielding is sensitive to the hydrostatic component of stress in addition to the shear component. The von Mises criterion is therefore not realistic, and alternative criteria are considered in the next sections.

The linear Drucker-Prager criterion

A simple modification of the von Mises criterion that includes hydrostatic stress sensitivity follows from equation (4)

$$\sigma_e = \sigma_o - \mu\sigma_m \tag{12}$$

Here σ_o is a material parameter which is now related to the shear yield stress σ_S by

$$\sigma_o = \sqrt{\sigma_S} \tag{13}$$

And σ_m is the hydrostatic component of stress given in terms of principal stresses by

$$\sigma_m = \frac{1}{3}(\sigma_1 + \sigma_2 + \sigma_3) \tag{14}$$

Equation (12) is identical to the linear Drucker-Prager model in the finite element package Abaqus where the notation used is

$$t - p\tan\beta = d \tag{15}$$

where t = σ_e, p = $-\sigma_m$, tan β = μ and d = σ_o. β is termed the friction angle.

The parameter μ depends on the adhesive material and characterises the sensitivity of yielding to hydrostatic stress. A value for μ can be determined from tests under two different stress states, and procedures for this are described in Chapter 4. Using yield stresses from shear and tensile tests

$$\mu = 3\left[\left(\sqrt{3}\,\sigma_S/\sigma_T\right) - 1\right] \tag{16}$$

From shear and compression data

$$\mu = 3\left[1 - \left(\sqrt{3}\sigma_S/\sigma_C\right)\right] \tag{17}$$

and from compression and tension data

$$\mu = \frac{3\left[(\sigma_C/\sigma_T) - 1\right]}{\left[(\sigma_C/\sigma_T) + 1\right]} \tag{18}$$

It should be noted that the above yield stresses σ_C, σ_T and σ_S are associated with the same effective plastic strain (see equation (26)).

Associated flow

The calculation of plastic strain components is achieved in plasticity theory using the flow rule in which increments of plastic strain are related to a plastic flow potential F by the equation

$$d\varepsilon_{ij}^p = d\lambda\frac{\partial F}{\partial \sigma_{ij}} \tag{19}$$

where $d\lambda$ is a factor that depends on stress state and is determined by ensuring equivalence of the plastic work done under all stress states using the expression

$$\sigma_e d\varepsilon_e^p = \sigma_{ij}d\varepsilon_{ij}^p \tag{20}$$

where σ_e and ε_e^p are the effective stress (equation (3)) and effective plastic strain (equation (26)) respectively.

For some materials, the flow potential F can be identified with the yield function, in which case the flow is said to be associated and from equation (12)

$$F = \sigma_e + \mu\sigma_m - \sigma_o \tag{21}$$

This relationship is valid if the resultant of the strain increment during flow is directed normal to the yield surface. The validity of this assumption for adhesives needs to be verified and a more general expression for F is based on non-associated flow.

Non-associated flow

Under non-associated flow, a more general expression for F is

$$F = \sigma_e + \mu' \sigma_m - \sigma_o \qquad (22)$$

The flow parameter μ' is then a material parameter that must be measured.

From equations (19) and (22), it follows that

$$\mu' = \frac{3(1 - 2v^p)}{2(1 + v^p)} \qquad (23)$$

Where v^p is the plastic component of Poisson's ratio determined under uniaxial tension and is given by

$$v^p = \frac{-\varepsilon_t^p}{\varepsilon_T^p} \qquad (24)$$

In Abaqus the flow potential, G, by analogy with equation (22) is

$$G = t - p \tan\Psi \qquad (25)$$

where $\tan\Psi$ has replaced μ'. Ψ is termed the dilation angle. If the calculated value of parameter μ' is not equal to μ then flow is termed non-associated. Associated flow is obtained by setting μ' equal to μ.

An effective plastic strain ε_e^p is defined in terms of principal plastic strains ε_i^p by

$$\varepsilon_e^p = \frac{\sqrt{2}}{3}\left[\left(\varepsilon_1^p - \varepsilon_2^p\right)^2 + \left(\varepsilon_2^p - \varepsilon_3^p\right)^2 + \left(\varepsilon_3^p - \varepsilon_1^p\right)^2\right]^{1/2} \qquad (26)$$

Effective plastic strains in shear, tension and compression are therefore given by

$$\varepsilon_e^p = \frac{2\varepsilon_S^p}{\sqrt{3}} = \frac{\gamma^p}{\sqrt{3}} = \frac{2}{3}\varepsilon_T^p(1+\nu^p) = \frac{2}{3}\varepsilon_C^p(1+\nu_C^p) \qquad (27)$$

where ν_C^p is the plastic component of Poisson's ratio measured in compression and $\varepsilon_S^p, \varepsilon_T^p$ and ε_C^p are plastic strains measured in shear, tension and compression. γ^p is the plastic shear strain measured in a shear test and is equal to twice the tensor component ε_S^p. Also, it should be noted that the compressive strain ε_C^p has a negative value. Relationships between ν^p and ν_C^p and the flow parameter μ' can be derived from the flow law, equation (19). Thus, for the linear Drucker-Prager model

$$\nu^p = \frac{3-2\mu'}{2(3+\mu')} \qquad (28)$$

and

$$\nu_C^p = \frac{3+2\mu'}{2(3-\mu')} \qquad (29)$$

It then follows from equation (27) that

$$\varepsilon_e^p = \frac{\varepsilon_T^p}{(1+\mu'/3)} = \frac{\varepsilon_C^p}{(1-\mu'/3)} \qquad (30)$$

The flow behaviour of adhesives is generally non-associated. Non-associated flow results in a nonsymmetrical stiffness matrix and negative eigenvalues can occur even when the hardening data doesn't show softening. When an analysis reaches such a bifurcation point, an implicit solver may have difficulty converging. For simplicity, associated flow can be assumed by setting $\mu = \mu'$ but the resulting loss in the accuracy of stress and strain calculations will be uncertain.

It should be mentioned here that the linear Drucker-Prager model is not capable of accurately describing the non-linear behaviour of an important class of tough adhesive, the rubber-toughened materials.

The exponent Drucker-Prager criterion

Although the linear Drucker-Prager yield criterion includes some sensitivity of yielding to the hydrostatic stress, it is not able to describe behaviour with any accuracy under stress states in which there is a high component of hydrostatic tension. Such stress states are common locally in adhesive bonds because of the high constraint imposed by the adherend under forces directed normal to the interface. An alternative criterion is significantly more accurate under these conditions and is often written in the form

$$\sigma_e^2 = \lambda\sigma_T^2 - 3(\lambda - 1)\sigma_T\sigma_m \tag{31}$$

where λ is another hydrostatic stress sensitivity parameter and relates stresses σ_C, σ_S and σ_T under uniaxial compression, shear and uniaxial tension by the equations

$$\lambda = \frac{\sigma_C}{\sigma_T} \tag{32}$$

$$\lambda = \frac{\sigma_C^2}{3\sigma_S^2} \tag{33}$$

and

$$\lambda = \frac{3\sigma_S^2}{\sigma_T^2} \tag{34}$$

In Abaqus the yield function is expressed as

$$F = aq^b - p - p_t = 0 \tag{35}$$

For the exponent form of the Drucker-Prager model with the exponent parameter, b, set equal to 2. The yield criterion equation (31) is then expressed as

$$aq^b = p + p_t \tag{36}$$

Similarly to the linear Drucker-Prager model, q = σ_e and p = $-\sigma_m$, so it follows that

$$a = \frac{1}{3\sigma_T(\lambda - 1)} \quad \text{and} \quad p_t = a\lambda\sigma_T^2 \tag{37}$$

If the flow potential F is associated with the yield potential, it takes the form

$$F = \sigma_e^2 - \lambda\sigma_T^2 + 3(\lambda - 1)\sigma_T\sigma_m \, p_t \tag{38}$$

Non-associated flow can be modelled by allowing λ to take an alternative value λ' (cf. equation (22)) which could be determined experimentally through measurement of Poisson's ratio in tension or compression. In Abaqus the exponent Drucker-Prager model only models non-associated flow. The expression for calculating λ' can be derived by substituting equation (38) with λ replaced by λ' into equation (19). It should however be noted that a hyperbolic function has been chosen for the flow potential F. The asymptote of the hyperbola coincides with the flow potential for the linear Drucker-Prager model, equation (25). The relevant material parameter in the flow law is therefore $\tan\psi = \mu'$ which can be calculated using equation (23).

Applicability to rubber toughened adhesives

If the materials models described above are used to analyse data from uniaxial compression, tension and shear, some limitations of the models are revealed. Figure 2 compares experimental data for true yield stress against true plastic strain measured on the rubber-toughened adhesive. Stresses and strains from the shear test have been scaled as shown to facilitate comparisons between the curves. When compared with the curve derived from a shear test, the data under compression and tension reveal a dependence of yielding on the hydrostatic component of stress. This is typical for this type of material and demonstrates that the von Mises criterion is inaccurate.
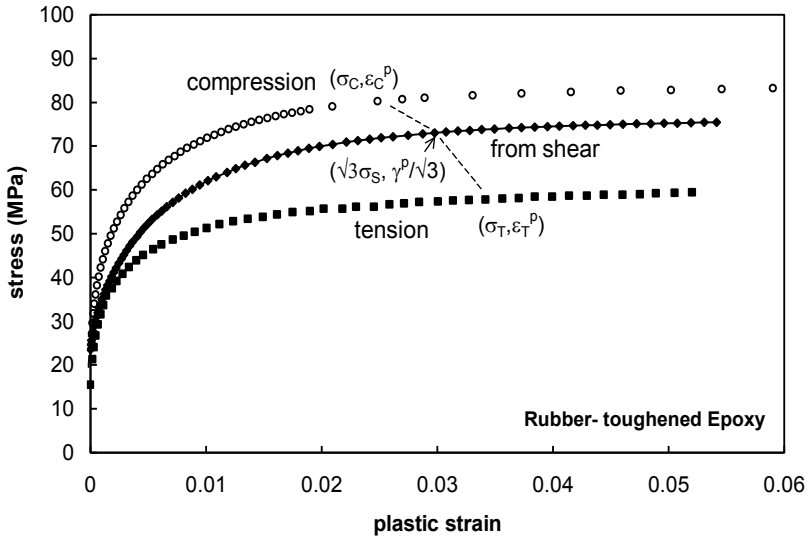
Figure 2. Comparison of stress/plastic strain curves determined under uniaxial tension, shear and uniaxial compression for the determination of stresses at the same effective plastic strain. Stresses and strains from shear data have been scaled as shown to facilitate comparisons between the curves.
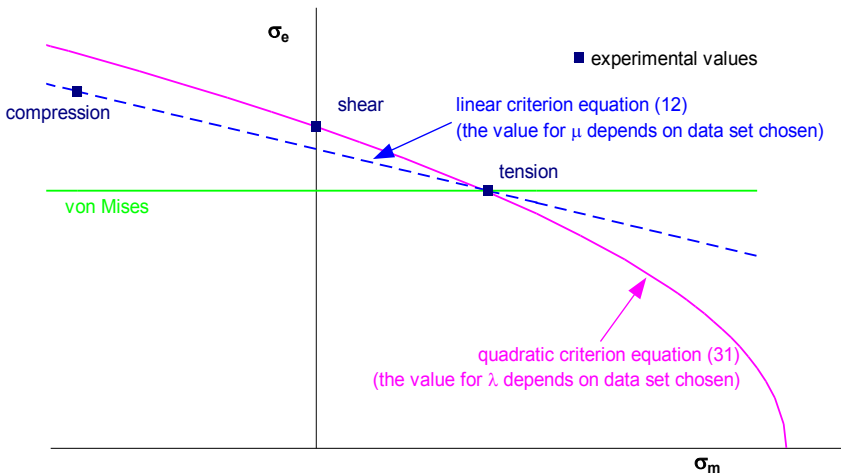

Figure 3. Plot of equivalent stresses under tension, shear and compression at an effective plastic strain of 0.03 on axes of effective shear stress σ_e against hydrostatic stress σ_m.

The hydrostatic stress sensitivity parameters μ and λ can be determined from data measured under two different states of stress (see equations (16) to (18) and (32) to (34)). The derived values for these parameters, however, depend upon which test data are selected. This is illustrated in Figure 3 which shows measured yield stresses obtained from the curves in Figure 2 and plotted on axes of deviatoric stress σ_e against hydrostatic stress σ_m (see equations (3) and (14)). The yield stresses were determined at an effective plastic strain (equation (27)) of 0.03. Figure 3 allows direct comparison of experimental data with the yield criteria in equations (4), (12) and (31). The inadequacy of the von Mises criterion is immediately apparent. The parameter μ in the linear Drucker-Prager criterion is the gradient of the line joining two data points, and this gradient is seen to be dependent on the data pair selected. Similarly, the value for the parameter λ derived for the quadratic criterion (exponent Drucker-Prager) also depends on the data set selected. These curves also indicate the need for experimental points at large hydrostatic stresses in order to fully characterise the yield surface. The butt-joint tension test described in Chapter 3 can provide such data.

These inconsistencies between measured and predicted behaviour for the rubber-toughened epoxy can be explained by the nucleation of cavities in the rubber phase. The nucleation of cavities requires a dilatational stress component and does not therefore occur under shear or compression. Its effect is to lower the tensile yield stress relative to the shear or compression stresses. Furthermore, cavitation creates the additional volumetric strain under tension which gives rise to a decrease in Poisson's ratio with plastic strain.

Material models which include the influence of void nucleation on ductility do not currently exist in FE packages. It is possible to include adaptations to elastic-plastic models through the use of a user subroutine. A model has previously been developed at NPL to include the effect of void nucleation on ductility through adaptations to existing elastic-plastic models. A detailed description of this cavitation model has been reported in the literature [1-4].

Rate-dependent plasticity

Both the linear and non-linear properties of adhesives are dependent on the rate at which the adhesive is deformed. A proper description of rate-dependent behaviour is needed for accurate calculations of strain distributions and performance under impact loading. The dependence of elastic properties on strain rate has been discussed briefly earlier in this chapter and is small enough to be negligible for glassy adhesives that are at temperatures well below their glass-to-rubber transition. Rate-dependent plasticity is accommodated in finite element systems through the presentation of hardening curves that vary with plastic strain rate. The measurement of these curves is described in Chapter 3. Data up to a maximum strain rate of around 10 s^{-1} can be measured using these tests. Data for rates above this are best determined by extrapolation. For this purpose, hardening curves can be modelled using the function

$$\sigma_T = \left[\sigma_y + (\sigma_f - \sigma_y)(1 - \exp - (\varepsilon_T^p/\varepsilon_r)^n)\right](1 + \alpha\varepsilon_T^p) \tag{39}$$

where σ_y, σ_f, ε_r, n and α are parameters which are chosen to give the best fit to experimental data. For the toughened epoxy used to illustrate results in this Guide, the yield stress parameters σ_f and σ_y are the only ones that vary significantly with plastic strain rate, and this dependence can be modelled using the relationships

$$\sigma_f = \sigma_{fo}(1 + b \log \dot{\varepsilon}_T^p) \tag{40}$$

and

$$\sigma_y = \sigma_{yo}(1 + c \log \dot{\varepsilon}_T^p) \tag{41}$$

where σ_{fo}, σ_{yo}, b and c are parameters determined from linear fits to plots of σ_y and σ_f against log plastic strain rate.

Chapter 3

Measurement of the properties of adhesives for FEA

- Data requirements
- Bulk specimen tests
- Joint specimen tests

Data requirements

Table 1 summarises the data needed for the different types of analysis described in Chapter 2. Much of the data requirements have been expressed in terms of tensile data, and these can be measured accurately and conveniently using standard test methods for plastics if bulk specimens are available. For some models, additional data are needed from compression or shear tests, and these can also be determined using bulk specimens as described in the following sections. Methods for preparing bulk specimens of adhesives have been described in ISO standards [5] and a Good Practice Guide [6].

For some adhesives, it is difficult or impossible to prepare bulk specimens of suitable size for testing. For other materials, there may be some concern over whether bulk specimen properties accurately represent the properties of the thin layer of the adhesive in a bonded joint. The characterisation of these materials can be achieved using joint specimen tests. The most appropriate ones for determining data for finite element analysis are described in this chapter. With joint tests, a lower accuracy in property measurement is usually obtained because of the very small gauge length (the bond thickness) of the specimen available for the measurement of strain.

Analysis	Type of behaviour	Data requirement
linear elastic		E and G or ν^e
linear viscoelastic	time or rate dependent	Stress relaxation modulus or creep compliance as a function of time
	frequency dependent	Dynamic modulus and loss factor as functions of frequency
elastic plastic	yielding not sensitive to hydrostatic stress	Elastic properties $\sigma_T(\varepsilon_T^p)$ or $\sigma_S(\gamma^p)$
	yielding sensitive to hydrostatic stress	Elastic properties $\sigma_T(\varepsilon_T^p)$ and $\sigma_S(\gamma^p)$ or $\sigma_C(\varepsilon_C^p)$ λ (=a) or μ (= tan β) λ' or μ' (= tan Ψ)
rate-dependent elastic-plastic		Same as elastic-plastic analyses and in addition $\sigma_T(\varepsilon_T^p, \dot{\varepsilon}_T^p)$

Table 1. Summary of data requirements for finite element analyses with different types of materials behaviour.

Bulk specimen tests

Tensile measurements

The modelling of dynamic or impact events requires the determination of elastic properties and hardening curves at various strain rates, covering the range of rates expected in the analyses. Standard electro-mechanical machines are suitable for determining data at strain rates up to 0.1 s^{-1}. Higher strain rates require a servo-hydraulic test machine [7].

Elastic properties are normally assumed to have little dependence on strain rate. Therefore, tensile tests [6] for the determination of Young's modulus and Poisson's ratio are carried out on standard specimens [8, 9] under constant deformation rate in a tensile test machine at relatively low strain rates. For best accuracy, contacting extensometers should be used for the measurement of axial and transverse strain, ε_T and ε_t. Two extensometers mounted on opposite faces of the specimen should preferably be used for the axial strain measurement to eliminate small non-uniformity in the strain through the thickness of the specimen caused by bending. The transverse strain measurement should be made close to the axial gauge section and, if possible, between the contact points of the extensometers. The contact pressure used to attach the extensometers to the specimen should be large enough to prevent slippage but insufficient to indent the specimen surface. Strain gauges are not recommended as they locally stiffen the specimen [6].

Values for Young's modulus and Poisson's ratio are calculated from the regression slopes in the linear region of the $\sigma_T - \varepsilon_T$ and $\varepsilon_t - \varepsilon_T$ curves. Use of regression slopes is preferable to single point values owing to the potential scatter in the data points (particularly the $\varepsilon_t - \varepsilon_T$ data) that is mainly due to uncertainties in the small extensions measured. Whilst elastic values can be determined over any strain range where the data appear linear, the slight curvature due to viscoelastic effects will tend to reduce the value of E as the strain range widens.

The measurement of tensile hardening curves involves use of the same tests out to larger strains. Contacting extensometers, unless they have been modified, typically have an upper strain limit of around 0.05. They may also initiate premature failure in the specimen at a point of contact. For these tests, the use of a video extensometer is therefore preferable for the measurement of axial strain. These instruments are generally unsatisfactory for the measurement of small displacements, so a contacting device is best used to measure the lateral strain for the determination of true stresses and the plastic component of Poisson's ratio. Normal video extensometers are limited to low rate tests owing to relatively slow sampling rates so a combination of contacting extensometers and crosshead movement is used to determine strains in higher rate tests. Standard test machine data loggers tend to

have too limited sampling rates to fully capture all the data points needed to determine stress-strain curves from high rate tests. Data capture using transient recorders or digital storage oscilloscopes can overcome this limitation. In high rate tests, errors in force measurement can result from resonance of the force transducer and the propagation of stress-wave pulses in the specimen. These errors can be reduced through the use of a piezo-electric force transducer and lightweight grips.

The dependence of strain hardening curves on strain rate $(\sigma_T(\varepsilon_T^p, \dot{\varepsilon}_T^p))$ is determined from tests carried out over a range of speeds. The acquisition of data at strain rates up to about 1 s^{-1} or possibly 10 s^{-1} is possible using the instrumentation described above. The measurement of strain generally causes problems at strain rates much above this, and there are no standard procedures for determining these data. Some experimental results up to a strain rate of 40 s^{-1} and the extrapolation of these to a rate of 1000 s^{-1} are discussed in the next section.

Illustrative data from tensile measurements

Figure 4 shows true tensile stress and Poisson's ratio data against true axial strain obtained from a tensile test on the toughened epoxy adhesive at a cross-head speed of 10 mm/min. In this test, the strain rate increased from 1x10^{-3} s^{-1} in the linear region to 2x10^{-3} s^{-1} at strains near the peak stress due to the specimen softening. The nominal strain rate of the test is taken as the strain rate near the peak stress. True stress and true strain values were derived using equations (5) and (6).

Figure 5 shows the variation of the tensile yield stress σ_T with the plastic strain ε_T^p derived from the data in Figure 4 using equation (7). These data constitute the tensile hardening curve $\sigma_T(\varepsilon_T^p)$ at the plastic strain rate of 2x10^{-3} s^{-1}.

Figure 6 shows how the hardening behaviour depends upon strain rate. The data at the strain rate of 40 s^{-1} were estimated from measurements of the cross-head displacement and a correlation between this and strain obtained from tests at lower speeds. The continuous curves are best fits to the data using equation (39) obtained using curve fitting software and enable the determination of hardening curves at higher strain rates by extrapolation using equations (40) and (41) [10].
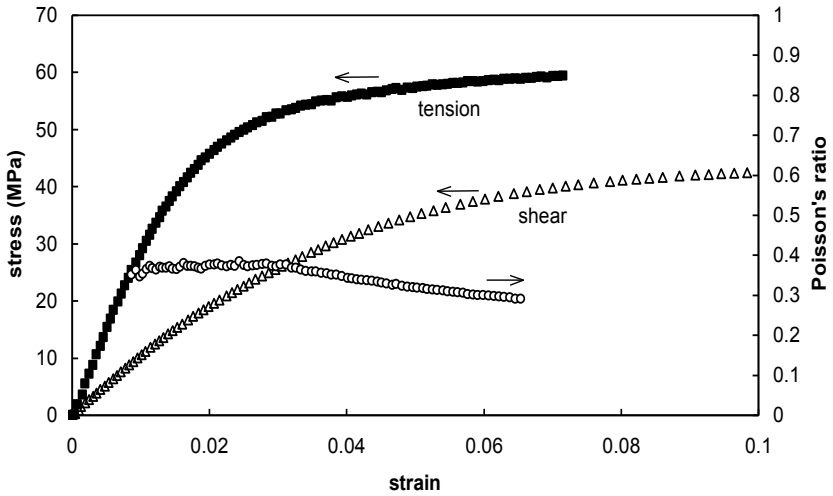
Figure 4. *Stress/strain curves and Poisson's ratio for the epoxy adhesive in tension and shear measured at the same effective plastic strain rate of 0.002 s^{-1}.*
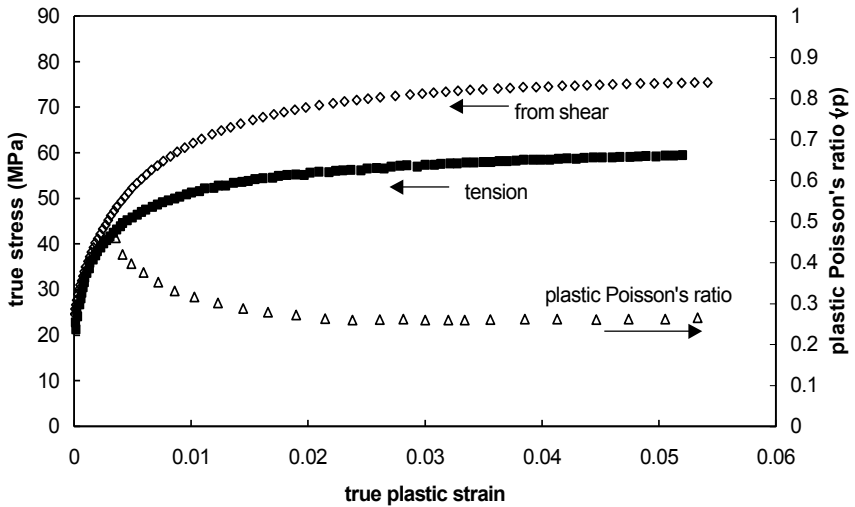

Figure 5. *Variation of tensile and shear properties with plastic strain used for the determination of parameters in elastic-plastic models.*
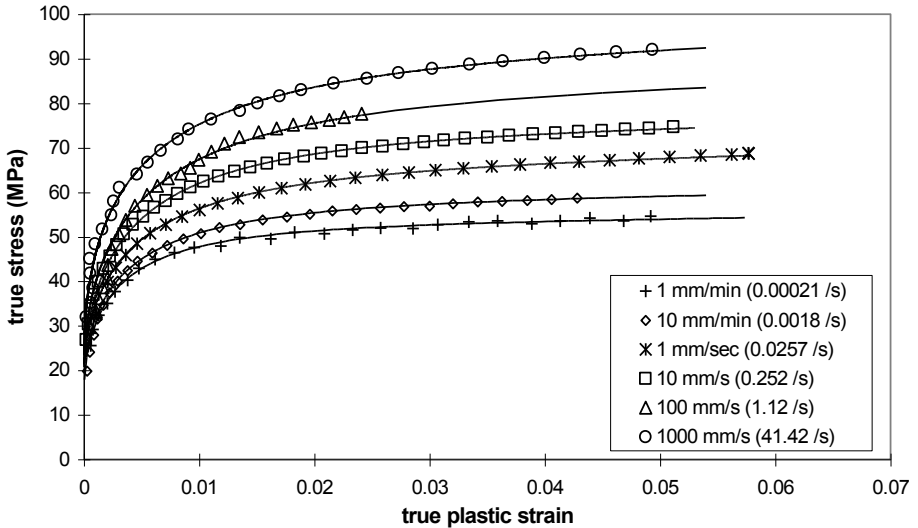
Figure 6. *Rate-dependent hardening curves for the epoxy adhesive. The continuous curves are fits to the data using equation (39).*

Shear measurements

Shear tests on bulk specimens can be carried out using the notched-plate shear (Arcan) [11] or notched-beam shear (Iosipescu) [12] methods. These methods are similar in that they use a double-notched specimen to achieve a region of predominantly pure shear in the centre of the specimen between the notches. Of these methods, the notched-plate shear test is probably the preferred one because the loading stage is simpler to construct, extensometers can be more conveniently used for strain measurement [13] and thinner test specimens can be employed. A schematic diagram of the specimen and loading arrangement is shown in Figure 7.

Specimen dimensions of 12 mm for the notch separation with a radius of the notches of 1.5 mm have been used successfully. A purpose-built extensometer [13] has been used for measuring the relative displacement of two points either side of a vertical line through the centre of the specimen. The separation of these points is 3 mm. Finite element analyses of the stress and strain distributions in the specimen reveal some non-uniformity in the shear stress between the notches and a small contribution to the measured displacements from

bending. These give rise to typical errors of about 7% in shear modulus and 2% in the shear flow stress.
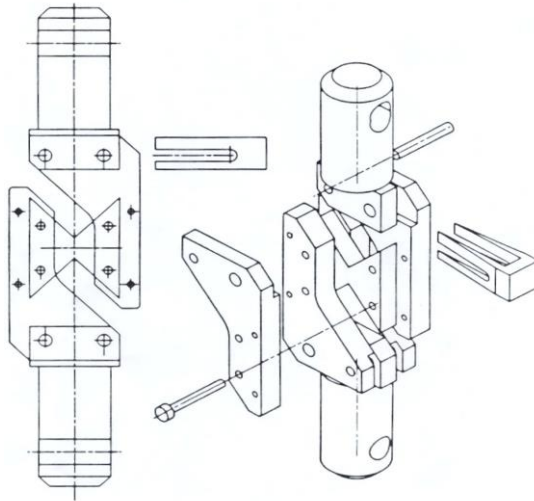

Figure 7. *Schematic diagram of apparatus for testing bulk specimens using the notched plate shear method.*

This test is unlikely to be suitable for brittle adhesives since a tensile failure will initiate near one of the notches before the full shape of the shear stress/strain curve is obtained.

Illustrative data from shear measurements

Figure 4 shows a shear stress/shear strain curve measured on the toughened epoxy using the notched-plate shear test. The test speed was 2 mm/min, and this gave a shear, plastic strain rate of 4×10^{-3} s^{-1}. The effective plastic strain rate (see equation (27)) is therefore about 2×10^{-3} s^1, which is comparable with that for the tensile test. Figure 5 shows the shear yield stresses in Figure 4 plotted against plastic strain. To aid comparison with the tensile results, the shear data have been plotted as $\sqrt{3}\sigma$ vs $\gamma^p/\sqrt{3}$. The differences between the shear and tensile yield stresses when plotted in this way illustrate the inadequacy of the von Mises yield criterion for modelling plastic deformation. It is worth noting that shear stress-strain curves generally show similar strain rate dependence to the tensile curves.

Compressive measurements

Measurements under uniaxial compression can be used instead of shear data to determine the sensitivity of plastic deformation to the hydrostatic component of stress and to derive the hydrostatic stress sensitivity parameter in the appropriate yield criterion. Furthermore, as explained previously, the results of measurements under tension, shear and compression can be used to assess the validity of candidate yield criteria.

Tests under uniaxial compression are difficult to perform because of the promotion of buckling of the specimen under high forces. The ISO 604 [14] standard test can be used to produce satisfactory results. This test employs short specimens with approximate dimensions 10 mm high x 10 mm wide. The thickness should be at least 3 mm and preferably higher. The top and bottom faces of the specimen must be machined smooth and accurately parallel. These are loaded in a testing machine between platens whose faces are smooth and accurately parallel. To minimise constraints by the platen surfaces to lateral expansion of the specimen during loading, the surfaces of the platens are lubricated with oil. Extensometers are used to measure changes in the platen separation, and nominal strain values are derived from the original specimen length. At small strains, errors in strain values arise through non-uniformity of the strain along the length of the specimen by this loading method. It is possible to apply a correction to these strains using a knowledge of Young's modulus from tensile tests. However, it is the properties under plastic deformation that are of most interest from this test. Plastic strains are derived using equation (7) with tensile stress and strain values replaced by compression values that are negative and with an apparent value for the Young's modulus under compression obtained from these tests. At small strains, uncertainties in plastic strains will be large but should become smaller at larger plastic strains.

Illustrative data from compression tests

Figure 2 compares the true stress/true plastic strain curve for the toughened epoxy under compression with curves measured under tension and shear. Data from these curves have been used in the section on Applicability to rubber toughened adhesives within Chapter 2, to assess the validity of elastic-plastic models for describing the non-linear behaviour of the toughened epoxy.

Joint specimen tests

Joint specimen tests offer the opportunity to test the adhesive in a form close to the form that it will have in the bonded structure. However, the accuracy and reliability of the materials properties obtained from joint specimen tests is reduced in comparison to bulk specimen tests because of higher uncertainties in strain resulting from small gauge lengths (normally the bond line thickness) and inclusion of adherend deformation in the measurement. It is also not possible to extract all of the required parameters (such as ν^p) from joint tests and assumptions concerning these parameters would need to be made when model predictions are made.

Shear property measurements

There are a number of joint-specimen tests that have been developed for determining the shear properties of adhesives. Some of these have been reviewed in reference [13]. Tests based on the torsion of butt-joint specimens are probably the most accurate but require special apparatus for load application and strain measurement. The relevant ISO standard is ISO 11003-1 [15]. The use of solid adherends leads to a variation of stress and strain across the specimen diameter and the need for data correction [16] to derive stress and strain values when the deformation is non-linear. The use of hollow, circular adherends avoids the need for this correction, but specimen preparation is more complicated.

The thick-adherend shear test is probably the most commonly used joint-specimen test for producing material properties under shear. An ISO standard (ISO 11003-2 [17]) exists for this test. The thick and specially profiled adherends in this test produce more uniform stress and strain distributions in the adhesive than are obtained in a lap-shear test. The latter should be used only for the acquisition of qualitative data on adhesive performance.
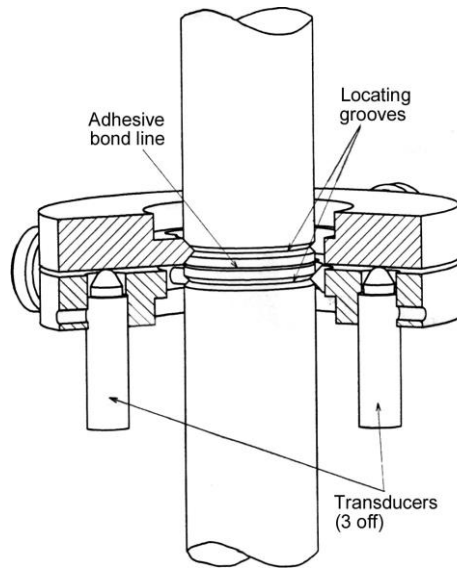
Figure 8. *Section detail of the extensometer for the butt-joint tensile test showing location grooves on the specimen.*

Tensile property measurements

Joint specimen tests are not used routinely for determining tensile property data for adhesives. Tensile tests on butt-joint specimens can however be used with suitable instrumentation to produce elastic properties and also plastic property results that serve to check the validity of elastic-plastic models. A suitable specimen geometry, together with extensometers for the measurement of strain in the adhesive, are shown in Figure 8. The specimen consists of two 25 mm diameter, cylindrical adherends that are bonded together at end faces. The V-shape groove in each adherend near the adhesive layer serves to locate an extensometer consisting of two rings with knife edges on their inner surfaces. Each ring locates in one of the grooves in the test specimen. One of the rings supports three precision displacement transducers that are equally spaced around the ring. The core of each transducer contacts the surface of the second ring. A value for the nominal axial strain in the adhesive under tension is determined from the average displacement divided by the adhesive layer thickness. A small correction can be applied for the contribution from the elastic deformation of the adherends to the total displacement recorded by the extensometer.

Accurate alignment of test specimen and loading assembly is critical in this test. The specimen is loaded through collet grips [18] that are rigidly mounted in the test assembly to minimise any lateral deformation of the specimen during loading. Without this constraint to lateral movement, the specimen is observed to bend during plastic deformation causing a non-uniform strain in the adhesive. An alignment fixture is used to position one grip and enable the specimen to be mounted precisely in the test assembly. The three individual displacement transducers provide a check on the axiality of the loading during the test. The readings will diverge should the specimen be misaligned.
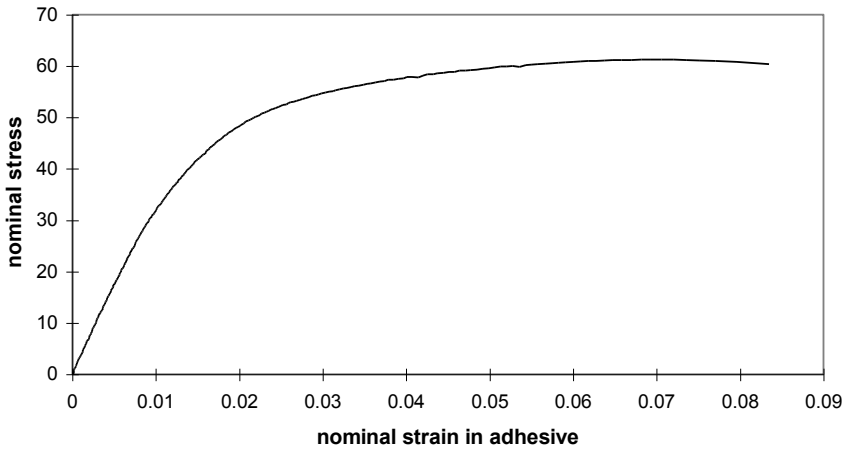

Figure 9. Stress/strain curve for a butt-joint specimen tested in tension.

Figure 9 shows a typical stress/strain curve for the toughened epoxy determined from a butt-tension test. Despite the large diameter-to-thickness ratio of the adhesive layer, the stress distribution in the adhesive is not strictly uniform so stress and strain data are nominal values. The slope of the curve in the region of small strains where behaviour is linear is the elastic modulus corresponding to the stress state where lateral stresses imposed by the adherends ensure that lateral strains are zero (in practice, only in the central region of the adhesive). The modulus under this stress state is

$$\frac{\sigma_a}{\varepsilon_a} = \frac{E(1 - v^e)}{(1 + v^e)(1 - 2v^e)} = K + \frac{4}{3}G \tag{42}$$

where σ_a and ε_a are the axial stress and strain respectively in the linear range of strain and K and G are the bulk and shear moduli respectively. Whilst this modulus value could be used with shear data from other joint-specimen tests to characterise elastic behaviour, it should be recalled that there is an uncertain error in this value arising from the non-uniformity of stress in the adhesive.

The data shown in Figure 9 can be used to assess the validity of a selected elastic-plastic model and associated parameters derived from tensile and shear or compression data. Predicted stress/strain curves for this test vary widely between the various models. The exponent Drucker-Prager model gives the closest agreement with experiment and predicts lateral stresses that increase to the value of the axial stress (implying pure hydrostatic tension) during plastic deformation. Other models predict lateral stresses that increase to values significantly less than this. This result suggests that stress and strain distributions calculated by the various models in regions of high peel stress will be significantly different and their accuracy is uncertain. This has hindered studies of failure in adhesive joint specimens and the development of a valid failure criterion (Chapter 6).

Chapter 4

Determination of model parameters for FEA

- Elastic properties
- Strain hardening functions
- Hydrostatic stress sensitivity factor μ
- Hydrostatic stress sensitivity factors λ and a
- Flow parameter μ'

This chapter describes the determination of property data and parameters required for stress analyses of joints and uses results on the toughened adhesives for purposes of illustration. The results of finite element analyses of some common joint geometries using these data are presented and discussed in the Appendix.

Elastic properties

Values for Young's modulus and the elastic component of Poisson's ratio were calculated from tensile stress/strain data obtained in the linear, low strain region, employing contact extensometers for the measurement of both longitudinal and transverse strains. Derived values are shown in Table 3.

Strain hardening functions

A tensile strain hardening function $\sigma_T(\varepsilon_T^p)$ is derived from a tensile stress/strain curve by subtracting the elastic component of strain from the total tensile strain (see Figure 1). Derived values for plastic strain are therefore sensitive to the value chosen for the slope of the linear region (nominally a Young's modulus). Since this quantity will depend upon test speed and experimental accuracy, it is recommended that elastic strains are determined using the best linear fit to the data being analysed. Stress/strain curves vary with strain rate, so analyses that take account of rate-dependent plasticity require hardening curves derived from tensile tests carried out over a range of loading speeds. These are shown in Figure 6.

Strain hardening data can be given in either single or multiple rate form. If a single strain rate hardening curve is used, this strain rate is assumed to be the average strain rate in the adhesive layer. The use of multiple rate hardening curves allows for regions of varying strain rate within the adhesive layer. Generally, four strain hardening curves separated by a factor of 10 in strain rate are used. One is chosen with a strain rate approximately the same as the average strain rate in the lap joint, one higher rate curve and one lower rate curve. An extremely low rate curve is also required and is designated the zero rate curve. Analysis difficulties can occur if more hardening curves are used or if too many data points are used to characterise each curve. The plastic strain value must always increase otherwise the analysis will not run. The best approach is to sample the hardening data until a representative curve is achieved. The sampling density of the hardening curves shown in Figure 6 has been used successfully.

The hardening curve data are required in the tabular form of yield stress with plastic strain where the first pair of numbers must correspond to the initial yield stress at zero plastic strain.

An example of hardening data is shown in Table 2. If strains in the analysis exceed the maximum effective strain supplied in the hardening curve, then the analysis will assume that additional extension occurs with no hardening. This can cause problems with successful convergence of the solution. One means of getting around this is to extrapolate a point on the hardening curve at a significantly higher strain using equation (39) or linear extrapolation of a supplied curve.

Yield stress (MPa)	Plastic strain
22.08	0
34.59	0.0004
45.48	0.0014
56.28	0.0034
65.98	0.0070
72.63	0.0120
76.89	0.0180
79.40	0.0240
81.05	0.0300
82.25	0.0360
83.18	0.0420
83.94	0.0480
84.58	0.0540

Table 2. Typical hardening curve data for a rubber-toughened epoxy at a strain rate of 3 s^{-1}.

Hydrostatic stress sensitivity factor μ = tan β

This parameter occurs in the linear Drucker-Prager model (see equations (12) and (15)) and is determined from yield stresses under two different stress states using equation (16), (17) or (18) depending on the tests chosen. Yield stress data under different stress states are shown in Figure 2. The yield stress values used for the calculation must be at the same effective plastic strain given by equations (27) or (30). If yield stress data are available in the plateau region of the stress strain curves, then yield stresses do not vary much with effective plastic strain. Accurate determinations of effective plastic strains are then not necessary. If this assumption cannot be made, effective plastic strains are derived from a knowledge of the plastic component of Poisson's ratio or the derived value for μ' from equation (23). As discussed in Chapter 2 and illustrated in Figure 3, the value obtained for μ depends upon which stress states are chosen. The value also depends on the plastic strain level chosen (a

further indication of limitations in the model) but this dependence becomes small at higher plastic strains. For the finite element analyses presented here, a value for μ was determined from the tensile and shear data in Figure 2 at an effective plastic strain of 0.03. From Figure 2 it can be seen that these values are located in the plateau regions of the shear and tensile data. The plastic Poisson's ratio, measured from the plateau of a ν^p versus ε^p plot (see Figure 5), was $\nu^p = 0.27$. Hence, from equation (27), values of ε_S^p and ε_T^p could be obtained. These values were:

$$\gamma_S^p = 0.052 \qquad \text{and} \qquad \varepsilon_T^p = 0.035$$

The relevant yield stress values could then be obtained from Figure 2 at $\varepsilon_T^p = 0.035$ and $\gamma_S^p = 0.052$, although as the shear data is plotted as $\gamma_S^p/\sqrt{3}$ then the yield shear stress value needs to be read from the graph at an effective plastic strain of 0.03. Thus:

$$\sqrt{3}\sigma_S = 73 \text{ MPa} \qquad \sigma_T = 58 \text{ MPa} \qquad \sigma_S = 42 \text{ MPa}$$

These yield stress values are the data, along with the plastic Poisson's ratio ν^p, required to calculate the Drucker-Prager parameters. The value for μ is then calculated from equation (16) so that:

$$\mu = 3\left[\left(\frac{73}{58}\right) - 1\right] = 0.78$$

Values for ν^p and μ are given in Table 3.

Hydrostatic stress sensitivity factors λ and a

These parameters are related and occur in the two versions of the exponent Drucker-Prager criterion equations (31) and (36). By selecting a pair of yield stresses at the same effective plastic strain from Figure 2, a value for λ can be calculated using equation (32), (33) or (34), and using equation (37) for the parameter a. In Abaqus, the flow potential assumed for this model is very similar to that used in the linear Drucker-Prager model (equation (25)). Effective plastic strains and the associated equivalent stresses may then be taken to be the same for the two models.

As described in the previous section, tensile and shear stresses at an effective plastic strain of 0.03 were selected for the determination of values for the parameters λ and a, which are recorded in Table 3.

The parameter λ is calculated using equation (34) as follows:

$$\lambda = \frac{(3 \times 42^2)}{58^2} = 1.58$$

The parameter a is then calculated using equation (37):

$$a = \frac{1}{[3 \times 58(1.58 - 1)]} = 0.0099$$

Flow parameter $\mu' = \tan \Psi$

The flow parameter was determined from the measured value of the plastic component of Poisson's ratio ν^p at an effective plastic strain of 0.03 using equation (23). The values for μ' and ν^p are given in Table 3. The parameter μ' is calculated from equation (23) where:

$$\mu' = 3(1-2 \times 0.27) / 2(1+0.27) = 0.54 \quad \mu = 3\left[\left(\frac{73}{58}\right) - 1\right] = 0.78$$

If experimental values for ν^p are not available, then associated flow can be assumed with $\mu' = \mu$. This will lead to some loss of accuracy in local stress and strain calculations as discussed in section A3 of the Appendix.

Parameter	Value
E (GPa)	2.97
ν^e	0.35
$\mu = \tan \beta$	0.78
λ	1.58
a (MPa^{-1})	0.01
ν^p	0.27
$\mu' = \tan \Psi$	0.54
$\sigma_T(\varepsilon_T^p)$ (MPa)	Fig 6

Table 3. *Materials properties and parameters used in finite element analyses of joints prepared with toughened epoxy.*

Chapter 5

Application of Finite Element Analysis

- Meshing
- Choice of solver
- Validity of FE predictions

Meshing

An element mesh is used to model the required geometry. The geometry needs to be modelled as accurately as possible, taking account of any symmetry, which would reduce the size of the model. One problem to be aware of when quantitatively analysing stress/strain predictions is the effect of geometric singularities i.e., sharp corners. In an elastic analysis, the stresses will go to infinity at the singularity. In an elastic-plastic analysis, stresses will only reach the plastic limit, but the predicted strains around the singularity will be unreliable, appearing much higher than expected. It is best to design both test-pieces and mesh geometry to remove geometric singularities by incorporating a radius on edges. If this is not possible, one should be aware of the unreliable predictions obtained in the small region surrounding a singularity. For example, the experimental joints modelled as part of recent work at NPL [10, 19] and illustrated in the Appendix (Figures A1 and A6) were prepared with radiused adherends, plus radiused fillets on the lap joint, to reduce stress concentrations. These radii were all included in the FE models to avoid singularities. Software such as Abaqus CAE [20] can be used to generate the geometry and mesh. It is best to apply boundary conditions and loads to features in the geometry as the mesh can then be changed at any time without having to alter the constraints. The boundary conditions and loads need to be applied carefully to duplicate the real situation as closely as possible.

Once the geometry has been created, an FE mesh can be applied to it. There are several factors to consider when meshing a geometry, such as element type, mesh density etc. The choice of elements can greatly influence results obtained from an analysis. In some cases, the difference in results between element types may not be visible in force/extension plots but observed in the stress or strain contours. There is a wide range of element families available in FE packages such as Abaqus [20], ranging from simple beam elements to solid (continuum) elements. There are also a variety of elements within each element family, each with their own advantages and disadvantages.

The elements used to model the adhesive joints mentioned above were solid (continuum) elements, which are suitable for linear analysis and also for complex nonlinear analyses involving plasticity and large deformations. There are a number of continuum elements available within the FE element libraries. The elements selected need to be appropriate for each particular analysis. For example, in a cylindrical butt joint specimen, axisymmetric elements can be used which represent the whole cylindrical structure with just one plane of elements. In the case of lap and scarf joints the adhesive layer would be modelled with quadrilateral elements rather than triangular elements as quadrilateral elements have a better convergence rate. Triangular elements could be used in small sections of the scarf joint adherends to mesh the angled sections of the joint. Quadrilateral elements perform best if their initial shape is approximately rectangular with a maximum aspect ratio of 7:1. The

elements become much less accurate when they are initially distorted. When modelling high loading rates e.g., in a lap joint analysis, the first order form of continuum elements is recommended. Second order elements are also available, and these provide higher accuracy than first order elements for 'smooth' problems that do not involve complex contact conditions of impact. Second order elements have more nodes per element than first order elements i.e., have a mid-side node. First and second order elements should not be mixed within a mesh without applying constraints, otherwise problems can be caused due to the different types of interpolation used within the two element types.

For structural applications, the FE element libraries, for two-dimensional continuum elements, include plane stress, plane strain and generalised plane strain elements. Plane stress elements can be used when the out-of-plane dimension of a body is small relative to its in-plane dimensions. The plane stress element assumes that the out-of-plane stress is zero. Modelling with this element generally applies to thin, flat bodies. In contrast, plane strain elements are generally used for modelling bodies where the out-of-plane dimension is much larger than the in-plane dimensions. In these elements it is assumed that the out-of-plane strains are zero. An alternative form of plane strain element is the generalised plane strain element. In this case the formulation used places the model between two rigid planes that can only move closer or further apart. It is assumed that the deformation of the model is independent of the axial position so the relative motion of the two planes causes a direct strain in the axial direction only. There are no transverse shear strains. Three-dimensional continuum elements avoid the artificial distinction between plane stress and plane strain. However, 3D elements normally lead to larger computational problems and hence, longer run times, so tend to be used less.

Another issue is the mesh density i.e., the number (and therefore size) of elements used within the mesh. It is general practice to run an initial analysis with a coarse mesh. Within the post-processing the deformed shape obtained should be checked to verify that the boundary conditions and loads are behaving as expected. From this analysis, force/extension data can be obtained and checked to make sure that they are physically reasonable. If this is the only required output, then it is not necessary to refine the mesh any further as this should not alter the force/extension behaviour of the model. But if localised stress or strain predictions are required then further mesh refinement is necessary. Mesh density can affect the strain (and stress) predictions in regions of strain (or stress) concentrations (see Appendix A2). A smaller element size will generally give a higher maximum value although at very small elements sizes further dimension changes should cause little effect (mesh convergence).

It is unnecessary to refine the whole mesh if there is only interest in quantitative predictions from areas of strain (or stress) concentration, and a highly refined mesh with high element density would lead to long analysis process times. With the coarse mesh, once satisfied that

the model is physically reasonable, contours of stress and strain can be plotted. These contours will highlight any area of interest that needs mesh refinement. The size of elements in this area should be reduced until a stable maximum value is achieved i.e., mesh convergence. Ideally, the peak stress or strain contour should be larger than the dimension of a single element (see contour plots in Appendix). In previous work it was found that, if too small an area of mesh is refined, strain localisations became 'trapped' within the refined mesh. Therefore, a reasonable area needs to be refined with gradually increasing element size out to a coarse mesh in areas where stress and strain values are relatively low and uniform. Once the mesh has been refined satisfactorily and the analysis run, post-processing should be used to check the continuity of stress contours. With averaged stresses plotted, the contours will look smooth. Unaveraged stresses should also be plotted (Quilt plot in Abaqus). If very discontinuous contours are observed, the mesh is no good for stress localisation investigations (although it would be suitable for obtaining force/displacements). When the mesh has been refined enough, even the unaveraged contours appear relatively smooth.

To recap on meshing issues, select the appropriate elements for the type of analysis. Use a coarse mesh for global loads/displacements. Use a refined mesh for localised stresses/strains, where one needs to be aware that singularities could artificially raise the predicted values.

Choice of solver

During an FE simulation, the numerical problem defined in an input file is solved using a mathematical code. The FE package Abaqus has a choice of solver codes. The standard (implicit) code can solve a wide range of linear and nonlinear problems. The explicit code is suitable for short, transient dynamic events, such as impact, and is also very efficient for highly nonlinear problems.

In nonlinear analyses the term "convergence" is used to indicate that the solution process for the nonlinear equation system converges. The solution at the end of an increment is, by definition, converged. If the solver cannot find a solution for a given increment of applied load, another attempt will be made to obtain a converged solution. When a new attempt is made, the solver cuts back the magnitude of the load increment. Several attempts may be used in any increment of the analysis. If too many attempts are made in a single increment, the solver terminates the analysis – the model has failed to converge. With the joint predictions, failure to converge is probably due to unstable material behaviour – the symptoms in these nonconvergence problems are most often divergence warnings. Convergence problems are less likely to occur if the model is loaded with applied displacements rather than applied loads.

A static analysis using the standard solver is the simplest form of elastic-plastic analysis. The models require a single tensile hardening curve for the adhesive material, thereby assuming an average strain rate in the adhesive layer. A static analysis is sufficient if only the long-term response of a structure to an applied load is of interest. However, if the duration of the applied load is short, a dynamic analysis should be performed. A dynamic analysis is one in which the inertia forces as well as rate-dependent plasticity are included in the dynamic equation of equilibrium.

In the FE package Abaqus, dynamic analyses can be carried out using either the standard (implicit) solver or the explicit solver. One limitation of using the explicit solver is that the time step is determined by the time for a stress wave to cross the smallest element dimension. The result is that processing times can be excessive, especially when a refined mesh is being used, or when the analysis is at a low loading rate. The processing time can be reduced by mass scaling i.e., using artificially high values of material density, but care must be taken to ensure that inertial forces still remain insignificant. The advantage with the standard solver is that the initial time increment size can be chosen manually. The automatic time incrementation scheme adjusts the increment size as necessary to obtain solutions. This means that the computer processing times are significantly shorter than when using the explicit solver, especially at the lower loading rates.

The explicit solver is particularly useful for analysing bonded joints made with tough adhesives that sustain large extensions before failure. The main advantage of the explicit code is that solutions can be obtained at larger extensions than with the standard dynamic analysis. This is illustrated in Figure 10, which compares standard dynamic analyses and standard quasi-static analyses for both linear and exponent Drucker-Prager models, and the explicit analysis using the linear Drucker-Prager model. A single hardening curve with a strain rate of 2.65 s^{-1} was used for each analysis, thereby assuming an average strain rate of 2.65 s^{-1} in the lap joint adhesive layer. It can be seen that the explicit dynamic analysis obtained solutions at higher extensions than the standard dynamic analysis. The standard dynamic analysis failed to obtain a solution at a smaller extension than the standard quasi-static analysis for both models. This failure is due to convergence problems.

A dynamic analysis can be used to consider the rate-dependent behaviour of adhesive properties. The accuracy of strain predictions is considered to be higher if a dynamic analysis is undertaken with rate-dependent hardening data i.e., multiple hardening curves, rather than a single strain rate hardening curve. This is because strain localisation, which is caused by enhanced softening of the adhesive in regions of high strain, is alleviated with rate-dependent data. This arises because the regions of high strain are also subjected to high strain rates, which increase the yield stress and reduce the strain softening associated with rate independent yielding.
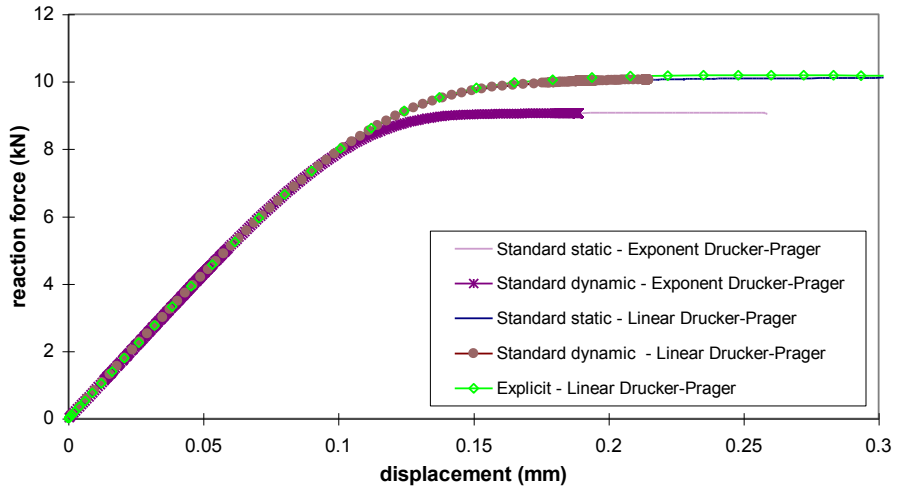
Figure 10. *Comparison of force/extension predictions obtained using both static and dynamic analyses. A single hardening curve obtained at a strain rate of 2.65 s^{-1} was used.*

When dynamic behaviour (with either single or multiple hardening curves) is modelled with an implicit solver, the analysis often fails at lower extensions. This may prevent predictions being obtained at the extensions of interest when investigating joint behaviour. The convergence problems appear to be due to unstable material behaviour. In the work illustrated in Figure 10, a single strain rate hardening curve was input for each analysis type. When a set of hardening curves was used, the standard dynamic analysis failed at extremely low extensions (~0.015 mm). This suggests that when modelling rate dependent adhesives, it may be necessary to use the explicit solver, with the associated increase in analysis time.

Variability of FE predictions

There are a number of choices made when first setting up an FE analysis that will affect the predictions obtained. This section gives a brief outline of the variability in predictions of localised strain and stress, illustrating that the choice of material model and analysis type can affect both the global loads/displacements and the localized stress and strain predictions. A more in-depth study is provided in the Appendix, covering predictions obtained from scarf and lap joint geometries in the form of force/extension curves and contour plots.

Mesh density can affect localised strain predictions. For example, a study on scarf joint behaviour showed a large increase in peak maximum principal strain as the element size was decreased (mesh density increasing). Although the force/extension curves predicted for both analyses were identical, the peak maximum principal strain for a coarse mesh was 0.193, increasing to 0.364 in a refined mesh.

The choice of materials model is of great importance, affecting both the force/extension curves and the stress and strain predictions. In the scarf joint study mentioned above analyses were carried out using Elastic, von Mises, linear Drucker-Prager and exponent Drucker-Prager materials models. Inspection of maximum principal strain and stress shows that the peak values vary greatly. The peak maximum principal strains range from 0.0569 for the elastic model to 0.364 for the exponent Drucker-Prager model. The peak maximum principal stresses go from 170 MPa for the elastic model to 62.3 MPa for the exponent Drucker-Prager model.

The choice of solver can also affect predictions. This was investigated during the study of a lap joint. It was found that, although all analyses followed the same force/extension curve, using an explicit code produced different strain and stress predictions e.g., a peak maximum principal logarithmic strain of 0.636 obtained using an implicit solver reduced to 0.592 if the explicit solver were used. The stresses also changed from 95.9 MPa to 97.1 MPa. Using multiple strain hardening curves with an explicit solver rather that a single curve decreased the peak maximum principal logarithmic strain values predicted from 0.592 to 0.462, though the predicted stresses decreased from 97.1 MPa to 94.7 MPa.

Criteria for joint failure

Criteria for joint failure

Adhesive joints fail by the initiation and growth of a crack. Depending on certain factors such as the adhesive type, the geometry of the joint and the load history, the growth phase can be rapid after crack initiation or slow until a critical crack length is reached for rapid fracture. A failure criterion defines a critical level of stress or strain, or a combination of these quantities, at which a crack will initiate. Since the crack in adhesive joints will initiate in a region of stress or strain concentration, which will generally be highly localised, the critical stress or strain level should ideally be determined in that region. Studies aimed at identifying a valid failure criterion therefore involve:

- measuring the force needed to initiate a crack in different geometries
- using a finite element analysis to predict the stress and strain components in the regions of maximum stress and strain where crack initiation is expected
- exploring various expressions of stress and/or strain that have a critical value at failure common to all joint geometries

Such studies are aided by simultaneous visual inspection to confirm the precise point and applied load corresponding to crack initiation. The failure criterion for untoughened thermosetting adhesives that exhibit little plasticity prior to a brittle failure in tension is likely to be based on a critical component of stress. On the other hand, tough adhesives that fail in a ductile manner after significant plastic deformation and flow (such as the toughened epoxy in Figure 4) are more likely to have a critical strain-based failure criterion. However, it should be noted that in many joint geometries, failure occurs in regions of high peel stress that have a relatively high component of hydrostatic stress and hence volumetric strain. These are conditions that are not simulated in a bulk specimen under uniaxial tension, and a criterion for failure of bulk specimens may not be appropriate to the failure of a bonded joint.

Probably the main factor inhibiting the identification of a failure criterion that is applicable to a wide variety of joint geometries is the ability to make accurate predictions of stress and strain components in the region where these are concentrated and where failure thus initiates. It is necessary to remove singularities in the analysis by imposing a radius on all edges and to use a suitably fine mesh to accurately represent the joint geometry, especially the shape of the fillets at the end of the bond. Even then, the results of analyses depend on the materials model used to describe the adhesive. This is illustrated in Figures A4 and A5 in the Appendix. These compare calculated distributions of the maximum principal stress and strain in a scarf joint obtained using four materials models. The stress and strain distributions predicted by the two Drucker-Prager models differ in both the magnitude of peak values and also in where these are located. In Chapter 2 of this Guide, it was demonstrated that neither of these models is able to accurately describe the deformation behaviour of this adhesive over all stress

states. This makes it difficult to determine, with sufficient confidence, stress and strain components responsible for the initiation of failure. The limitations of a chosen material model to represent a selected adhesive must be taken into account when using FEA to predict the initiation of failure.

Chapter 7

References

References

1. B.E. Read, G.D. Dean and D.H. Ferriss, An elastic-plastic model for the non-linear mechanical behaviour of rubber-toughened adhesives. NPL report CMMT(A)289, October 2000.

2. B. Read and G. Dean. Plastics, Rubber and Composites, (2001), 30, p 328.

3. G Dean and L Crocker. Plastics, Rubbers and Composites, Vol 36, No 1, Feb 2007, pp1-13; https://doi.org/10.1179/174328907X174575

4. L Crocker and G Dean. Plastics, Rubbers and Composites, Vol 36, No 1, Feb 2007, pp14-25; https://doi.org/10.1179/174328907X174584

5. ISO 15166:1998, Adhesives – Methods for preparing bulk specimens. Part 1: Two-part systems. Part 2: Elevated-temperature curing one-part systems.

6. G.D. Dean and B.C. Duncan, Preparation and Testing of Bulk Specimens of Adhesives. NPL Measurement Good Practice Guide No 17, July 1998.

7. B. Duncan, G. Dean and A. Pearce, Selection of test methods for determining the impact properties of adhesives. Proceedings of 7th International Conference on Adhesion and Adhesives (Adhesion '99), September 1999.

8. ISO 3167:2014, Plastics – Multipurpose test specimens.

9. ISO 527-2:2012, Plastics – Determination of tensile properties – Part 2: Test conditions for moulding and extrusion plastics.

10. G. Dean and L. Crocker, Comparison of the measured and predicted deformation of an adhesively bonded lap-joint specimen. NPL report CMMT(A)293, November 2000.

11. M. Arcan, Z. Hashin and A. Voloshin, Experimental Mechanics, vol 18 (1978) p141.

12. D.F. Adams and D.E. Walrath, J. Composite Materials, vol 21 (1987) p494.

13. G. Dean, B. Duncan, R. Adams, R. Thomas and L. Vaughn, Comparison of bulk and joint specimen tests for determining the shear properties of adhesives. NPL report CMMT(B)51, April 1996.

14. ISO 604:2002, Plastics – Determination of compressive properties.

15. ISO 11003-1:2019, Adhesives – Determination of shear behaviour of structural bonds. Part 1: Torsion test method using butt-bonded hollow cylinders.

16. R. Thomas and R. Adams, Test methods for determining shear property data for adhesives suitable for design. Part 2: The torsion method for bulk and joint test specimens. MTS Adhesives Project 1, Basic Mechanical Properties for Design. Report No 7 March 1996.

17. ISO 11003-2:2019, Adhesives – Determination of the shear behaviour of structural bonds. Part 2: Thick-adherend shear test method.

18. L. Crocker and G. Dean, Tensile testing of adhesive butt-joint specimens. NPL Measurement Note MATC(MN)09, May 2001.

19. G. Dean and L. Crocker, Analysis of joint tests on an epoxy adhesive. NPL report MATC(A)40, July 2001.

20. Abaqus 2021 user documentation, © 2009-2021, Dassault Systèmes Simulia Corp

Chapter 8

Appendix

- A1 - Application of FEA to some common joint geometries
- A2 - Analysis of a scarf joint
- A3 - Analysis of a lap joint

A1   Application of FEA to some common joint geometries

This appendix provides an illustration of the application of FEA to a scarf joint (section A2) and a lap joint (section A3). Both joints were assembled using the toughened epoxy adhesive used for illustration throughout this Guide. In both cases the results of analyses give a comparison of predicted maximum principal stresses and strains for a variety of analyses. The material parameters and properties used in these analyses are listed in Table 3. This examination of predictions obtained from analyses using various materials models for the scarf joint geometry and from different analysis types for the lap joint geometry highlight how the choice of material model and analysis type can affect both the global loads/displacements and the localized stress and strain predictions.

A2   Analysis of a scarf joint

For the scarf-joint specimen, adherends had an angle of 65° between the bond face and side of the adherend (see Figure A1). This angle was chosen as calculations indicated that it would produce an average strain state in the adhesive composed of roughly equal proportions of volumetric and shear components. The ends of the adherends have a radius of 1 mm to remove geometric singularities.

The FE results presented here have been obtained using various materials models, see Chapter 2. These models include the simple elastic model, and three variations of elastic-plastic model: the commonly used von Mises, the linear Drucker-Prager and the exponent Drucker-Prager. Figure A2 shows the force/extension curves obtained from analyses of the scarf joint using these four different models. A typical experimental curve is also shown for comparison. It can be seen that all models match the experimental curve initially, but that after this linear elastic region the predictions diverge. The elastic analysis continues in a linear manner, predicting increasingly high loads as the extension increases. The elastic-plastic models all exhibit non-linear behaviour but with varying degrees of accuracy. The von Mises model, which does not allow for hydrostatic stress sensitivity, over predicts the loads throughout the whole non-linear region. At the average failure extension for the scarf joint (0.035 mm) the von Mises predicted load is nearly 60% higher that the experimental load. Both the linear and exponent Drucker-Prager models allow for hydrostatic stress sensitivity, and this brings the predictions much closer to the experimental data, although the linear Drucker-Prager still slightly overestimates the load. The exponent Drucker-Prager prediction gives a good fit to the data. Two force/extension curves have been plotted for the exponent Drucker-Prager model. One was obtained using a coarse mesh, the other using a refined

mesh. The predictions correlate confirming that mesh density does not affect global force/displacement predictions.

The effect of mesh density on localised strain predictions is demonstrated in Figure A3. Figure A3 shows contour plots of maximum principal strain in the adhesive layer of the scarf joint for (a) a coarse mesh and (b) a refined mesh. Although the contour plots appear similar, the maximum principal strain predicted in the coarse mesh is 0.193 compared to 0.364 for the refined mesh. Refining the mesh has increased the local strain predictions.

All contour plots presented for the scarf joint analyses are obtained at an extension of 0.035 mm, which represents the average experimental failure extension. The contour plots of maximum principal strain from analyses using the refined mesh are shown for all four models in Figure A4. The elastic analysis (Figure A4(a)) gives a maximum principal strain of 0.0569, which is very small compared to the elastic-plastic analyses. For these analyses, the von Mises model (Figure A4(b)) predicts a maximum principal strain of 0.279 and the linear Drucker-Prager model (Figure A4(c)) gives a value of 0.148, while the exponent Drucker-Prager (Figure A4(d)) predicts the highest maximum principal strain, with a value of 0.364. The contour plots all look very different. For the exponent Drucker-Prager model with both the coarse and refined mesh, a localised zone of high strain has developed. This was seen to initiate close to the radius at the acute angle of the adherend at smaller extension, then grow through the thickness of the adhesive and is finally concentrated along the opposing interface. None of the other models produce a localised zone of this sort, although the von Mises and linear Drucker-Prager models both predict localised high strains along the interface with the lower adherend.

Figure A5 shows the maximum principal stress predictions obtained using the four material models. The elastic analysis (Figure A5(a)) gives a maximum principal stress of 170 MPa, which is much higher than the elastic-plastic predictions. The von Mises model (Figure A5(b)) predicts a value of 106 MPa, while the linear Drucker-Prager (Figure A5(c)) gives a maximum principal stress of 69.9 MPa. The exponent Drucker-Prager model (Figure A5(d)) produces the lowest maximum principal stress with a value of 62.3 MPa. In all cases, the maximum principal stress is highest in the adhesive away from the radius. Further investigation into stress predictions using the exponent Drucker-Prager model has shown that the hydrostatic stress (the average of the three principal components) is highest at the interface near the middle of the radiused region.
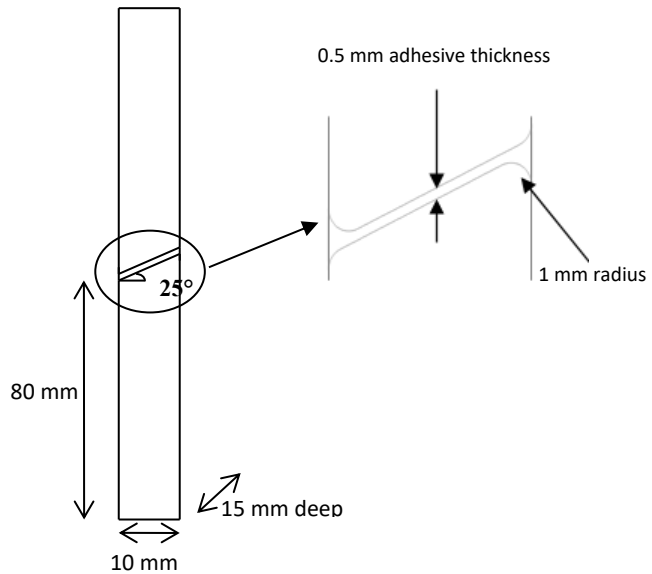
Figure A1. *Schematic diagram of the scarf-joint specimen showing the dimensions and the geometry of the adherends.*
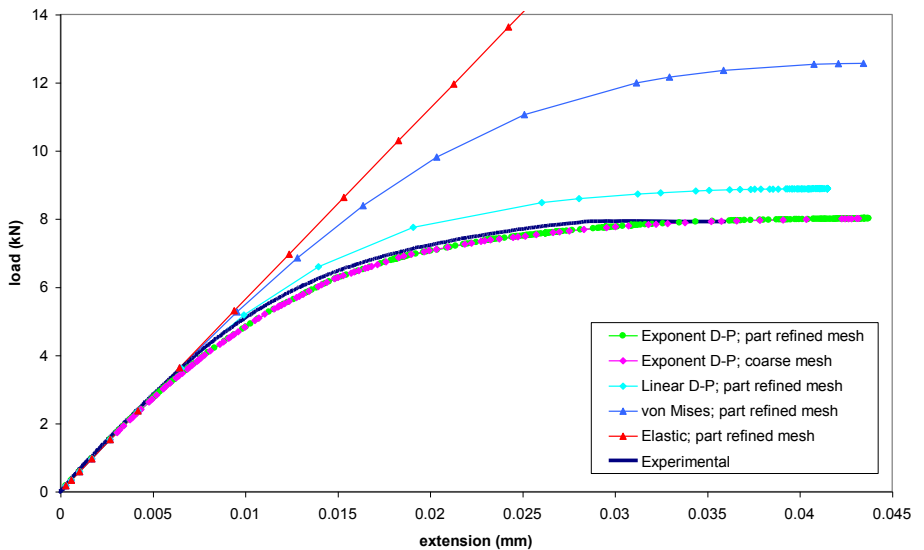

Figure A2. *Comparison of force/extension predictions of the scarf-joint specimen obtained using four material models and a typical experimental curve: quasi-static analyses using the standard solver.*
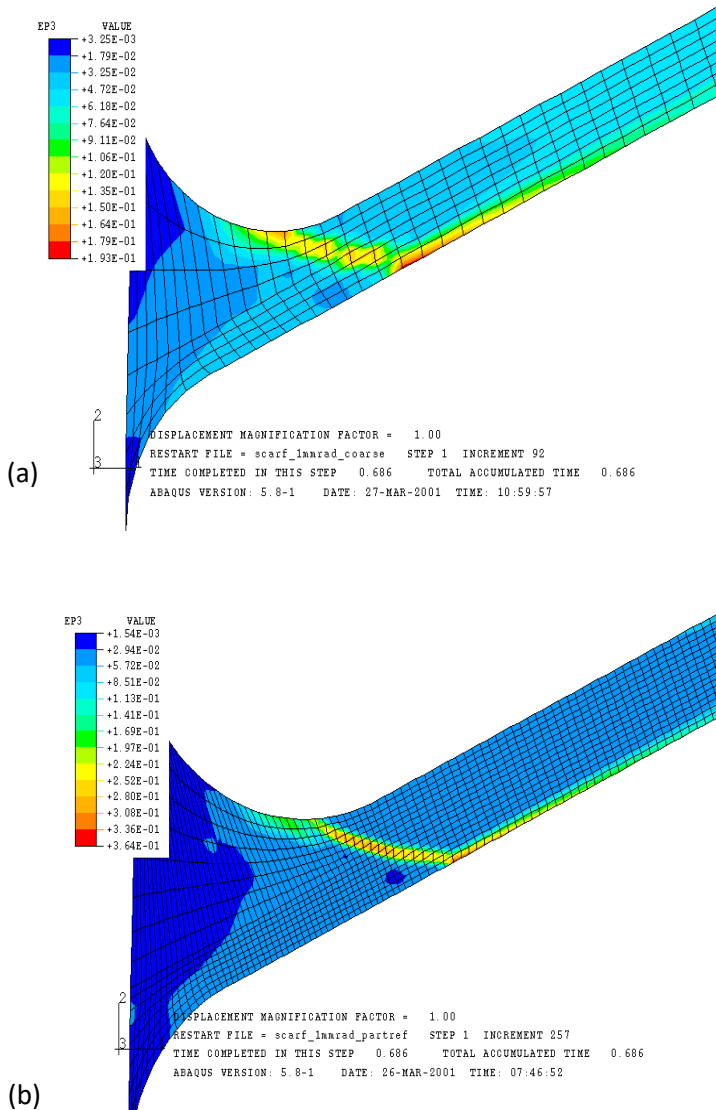
Figure A3. *Comparison of maximum principal strain predictions from (a) a coarse mesh and (b) a refined mesh. Exponent Drucker-Prager analysis: quasi-static analysis, standard solver.*
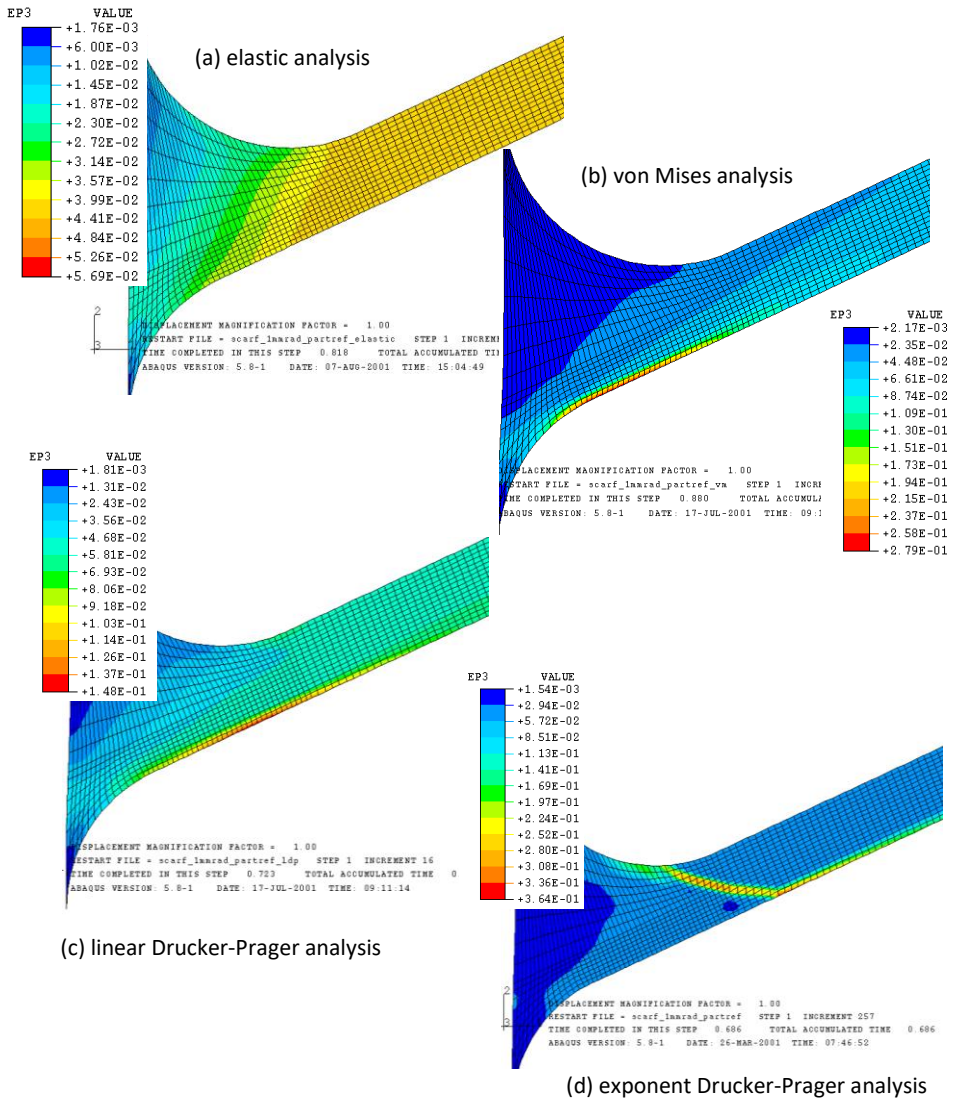
Figure A4. *Contour plots of maximum principal strain in the adhesive at an extension of 0.035 mm obtained from analyses using four different material models. Same data and analyses as Figures A2 and A3.*
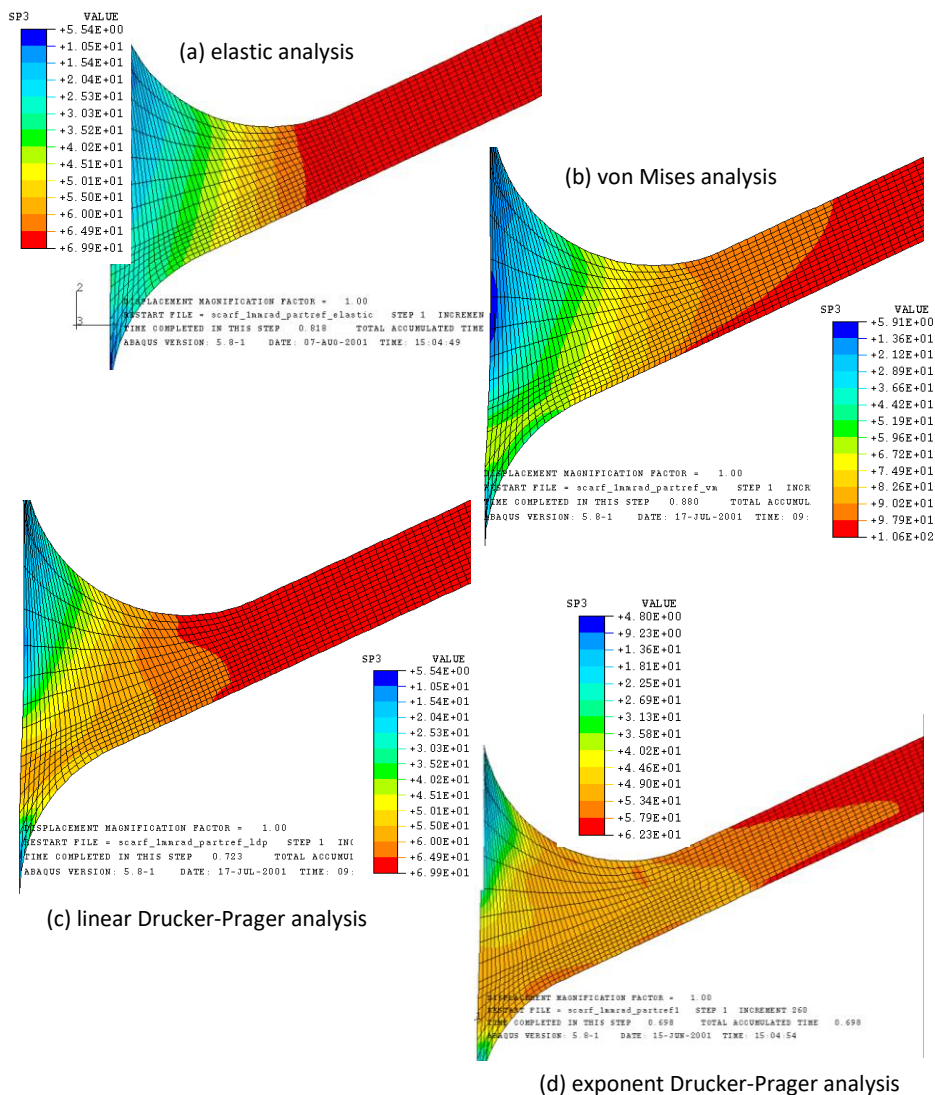
Figure A5. *Contour plots of maximum principal stress in the adhesive at an extension of 0.035 mm obtained from analyses using four different material models. Same data and analyses as Figure A4.*

A3   Analysis of a lap joint

Figure A6 shows a diagram of the lap joint specimen. Radii were included on the adhesive fillet and the end of each adherend within the bond to avoid geometric singularities. The FE results presented for the lap joint analyses have been obtained with the linear Drucker-Prager material model using a variety of analysis types and a test speed of 1 mm/s. The following analyses have been performed:

- static analysis with a single rate hardening curve (3 s^{-1}) using Abaqus/Standard
- dynamic analysis with a single rate hardening curve (3 s^{-1}) using Abaqus/Standard
- dynamic analysis with multiple rate hardening curves using Abaqus/Standard
- dynamic analysis with a single rate hardening curve (3 s^{-1}) using Abaqus/Explicit
- dynamic analysis with multiple rate hardening curves using Abaqus/Explicit

Figure A7 shows force/extension predictions for the five analyses. The extension refers to a 25 mm gauge length centred on the bonded region. It can be seen that all the analyses follow the same force/extension curve, although the standard dynamic analysis with multiple rate hardening curves failed to converge at a very small extension (~ 0.04 mm). The standard static/single rate, explicit/single rate and explicit/multiple rates analyses all reached the required extension. The standard dynamic analysis with single rate was stopped at an extension of 0.2 mm as it had taken 3000 increments to reach this point and had generated very large output files. The explicit, rate-dependent force/extension curve is very similar to those obtained using a single hardening curve at a strain rate of 3 s^{-1}. In earlier work [10] the curve at a strain rate of 3 s^{-1} was specifically chosen as a single 'effective' strain hardening curve for a test speed of 1 mm/s as it gave a comparable force/extension curve to that obtained from an analysis using four hardening curves at that loading speed. A lower, strain-rate hardening curve would lower the plateau load predicted for the joint and vice versa.

In both the scarf and lap joint analyses, the linear Drucker-Prager model has been run with non-associated flow i.e., the dilation angle ($\psi = \tan^{-1}\mu'$) does not equal the material friction angle ($\beta = \tan^{-1}\mu$), where ψ, β, μ' and μ are linear Drucker-Prager model parameters. In the Abaqus exponent Drucker-Prager model, flow is always non-associated. With the linear Drucker-Prager model, flow can be associated by setting $\psi = \beta$. The effect of this can be seen in Figure A7 where it is seen that the linear Drucker-Prager prediction with associated flow gives higher load predictions than the equivalent model with non-associated flow. The linear Drucker-Prager model with associated flow predicts higher maximum principal strains and lower maximum principal stresses in the adhesive than the equivalent model with non-associated flow. These differences in localized strain and stress predictions can be seen in

Figure A8 which shows contour plots of maximum principal strain for (a) non-associated flow and (b) associated flow and also Figure A9 showing contour plots of maximum principal stress for (a) non-associated flow and (b) associated flow, all obtained at an extension of 0.1 mm.

The following section examines the differences in localized strain and stress predictions within the lap joint adhesive using different solvers and single or multiple hardening curves. All results have been obtained with the linear Drucker-Prager model. Stress and strain distributions are obtained at an extension of 0.2 mm. In Abaqus/Explicit the only available principal strain output is the principal logarithmic (or true) strain (equation (6)); hence contour plots of maximum principal logarithmic strain have been obtained for all analyses, along with contour plots of maximum principal stress.

Figure A10 shows contour plots of maximum logarithmic principal strain for analyses run using a single rate hardening curve (3 s^{-1}) and different solvers. The standard static (a) and explicit (b) analyses produce very similar maximum principal logarithmic strains, with peak values of 0.636 and 0.592 respectively. The contour plots of maximum principal logarithmic strain show the same localized strain concentration near the radius of the adherend. Contour plots of maximum principal stress from the two analyses run with single rate hardening curves are shown in Figure A11. The maximum principal stress peaks at the interface with the adherend but slightly further around the radius than the location of the peak in the maximum principal logarithmic strain. Once again, the standard static and explicit analyses, Figure A11 (a) and (b) respectively, predict similar results with peak values of 95.9 MPa and 97.1 MPa. This implies that there is little difference between results obtained from standard and explicit analyses.

Figures A12 and A13 compare the predictions obtained from analyses using single rate hardening curves with those from rate dependent dynamic analyses (multiple rate hardening curves). Figure A12 shows contour plots of maximum principal logarithmic strain from (a) single rate and (b) multiple rate explicit analyses respectively. It can be seen that including rate dependent data lowers the peak values from 0.592 (single rate) to 0.462 (rate dependent). Figure A13 shows contour plots of maximum principal stress. It is apparent that the inclusion of rate dependent data decreases the peak values of maximum principal stress from 97.1 MPa (single rate) to 94.7 MPa (rate dependent). The selection of single or multiple rate hardening curves clearly has a significant effect on predictions of strain values.

These predictions of lap joint behaviour are for illustration only. Stresses and strains of these magnitudes would not be obtained experimentally as, at this extension, cracks would already have initiated in the adhesive layer.
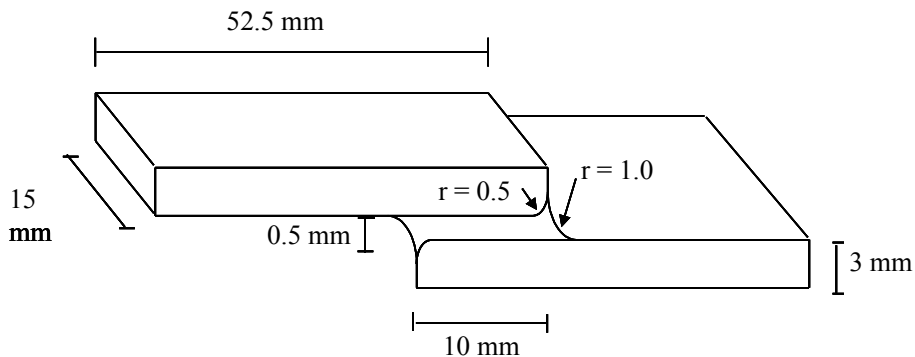
Figure A6. *Schematic diagram of the lap joint specimen showing radii on the adherends and adhesive.*
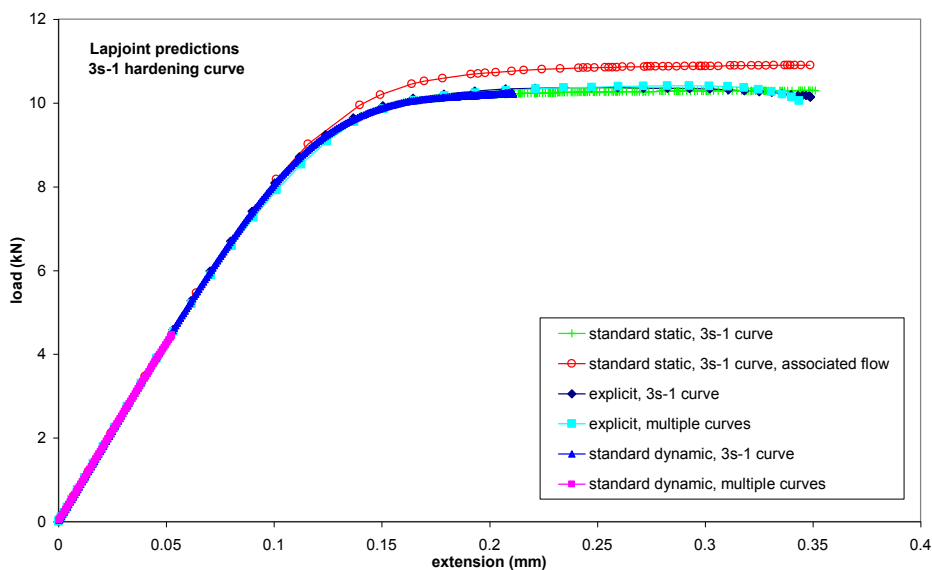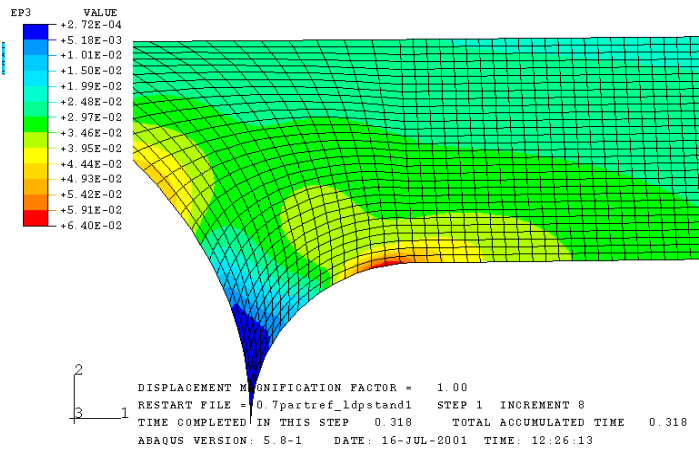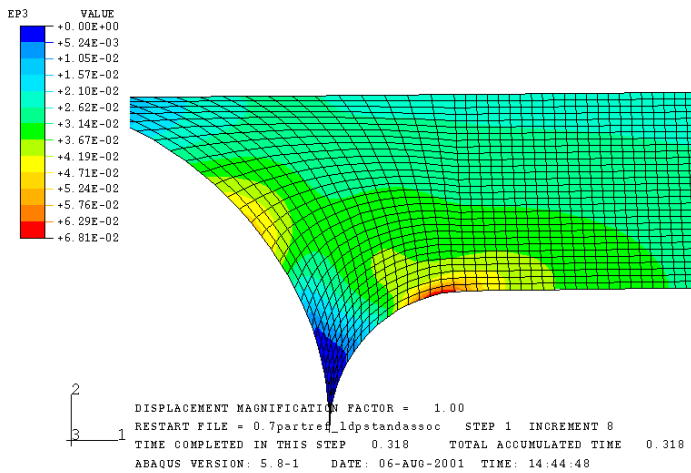

Figure A7. *Comparison of force/extension predictions of the lap joint specimen obtained using standard and explicit solvers and single rate and multiple rate hardening curves with the linear Drucker-Prager model.*
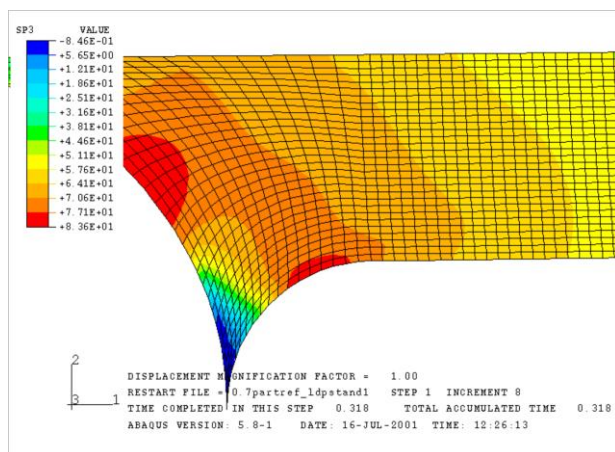
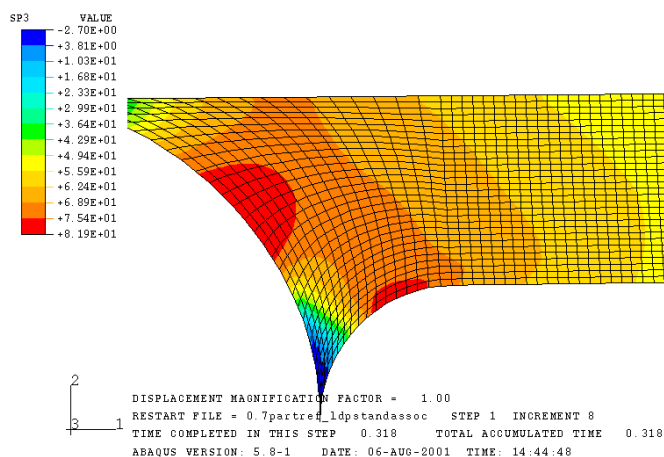(a) linear Drucker-Prager analysis with non-associated flow

(b) linear Drucker-Prager analysis with associated flow

Figure A8. *Contour plots of maximum principal strain showing localised strain and stress predictions obtained using the linear Drucker-Prager model with either (a) non-associated or (b) associated flow, using Abaqus/Standard at an extension of 0.1 mm.*
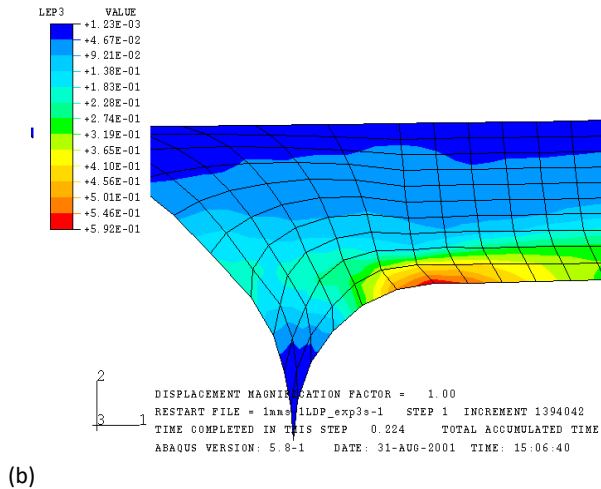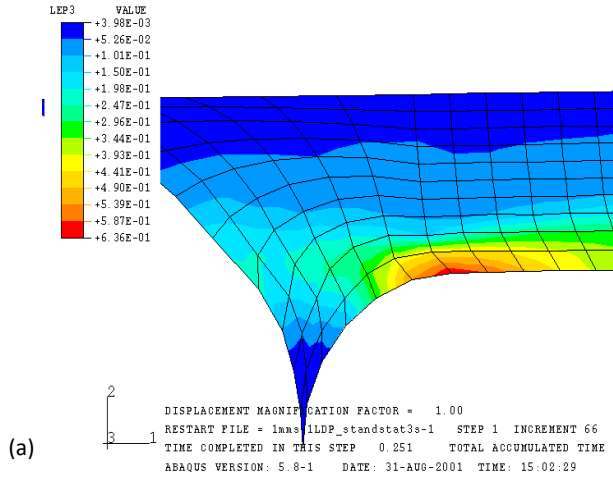
(a) linear Drucker-Prager analysis with non-associated flow

(b) linear Drucker-Prager analysis with associated flow

Figure A9. *Contour plots of maximum principal stress showing localised strain and stress predictions obtained using the linear Drucker-Prager model with either (a) non-associated or (b) associated flow, using Abaqus/Standard at an extension of 0.1 mm.*

Figure A10. *Contour plots of maximum principal logarithmic strain at an extension of 0.2 mm for two different analyses: (a) standard static and (b) explicit. Both analyses run with the linear Drucker-Prager model and a single rate hardening curve (3 s^{-1}).*
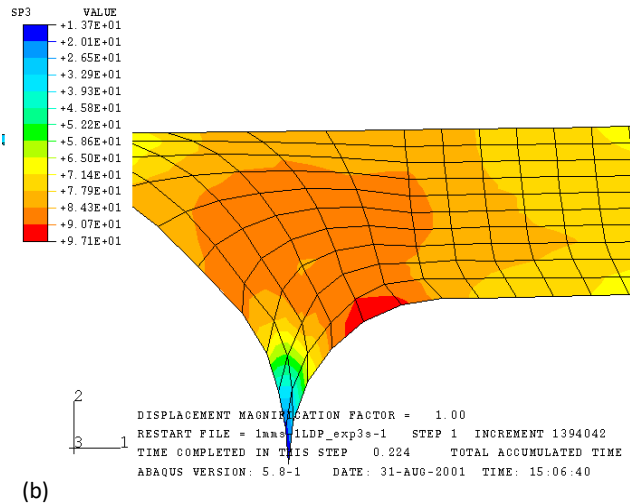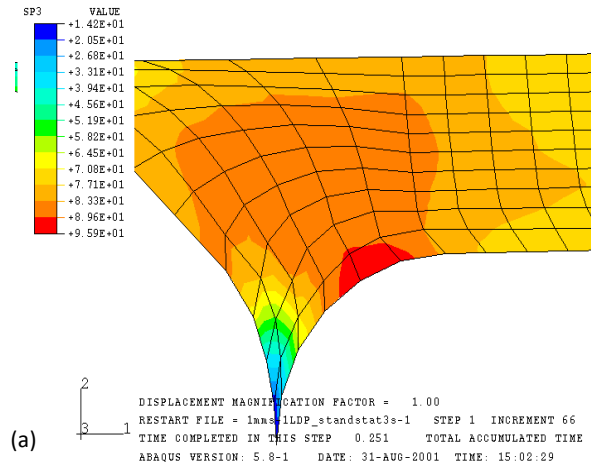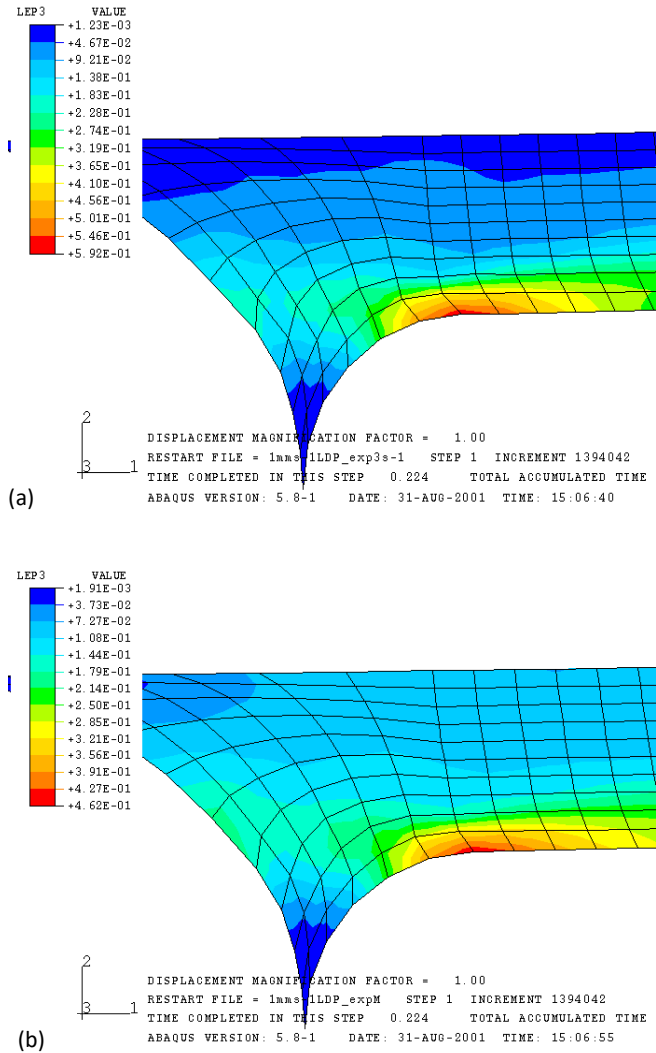
Figure A11. *Contour plots of maximum principal stress at an extension of 0.2 mm for two different analyses: (a) standard static and (b) explicit. Both analyses run with the linear Drucker-Prager model and a single rate hardening curve (3 s⁻¹).*

Figure A12. *Contour plots of maximum principal logarithmic strain in the adhesive at an extension of 0.2 mm obtained from an explicit analysis using (a) a single rate hardening curve (3 s⁻¹) and (b) multiple rate hardening curves. Linear Drucker-Prager model.*
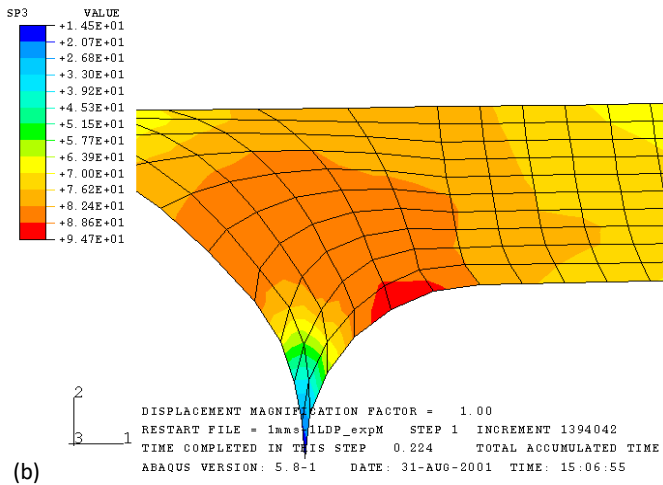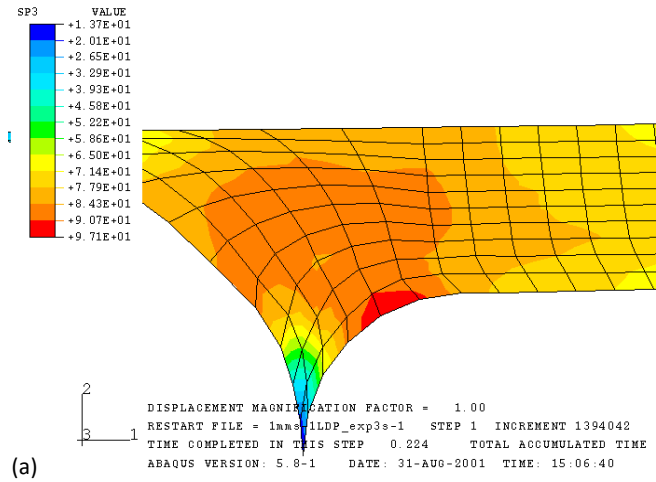
Figure A13. *Contour plots of maximum principal stress in the adhesive at an extension of 0.2 mm obtained from an explicit analysis using (a) a single rate hardening curve (3 s^{-1}) and (b) multiple rate hardening curves. Linear Drucker-Prager model.*